ENGINEERING EXPERIMENT STATION
DEPARTMENT OF MECHANICAL
AND INDUSTRIAL ENGINEERING
ME-TN-036-1

THEORETICAL STUDY OF RADIANT HEAT EXCHANGE FOR NON-GRAY NON-DIFFUSE SURFACES IN A SPACE ENVIRONMENT

By
R. G. HERING

Research Sponsored by
NATIONAL AERONAUTICS AND SPACE ADMINISTRATION
under Grant NGR-14-005-036
FINAL REPORT

UNIVERSITY OF ILLINOIS
URBANA, ILLINOIS
SEPTEMBER, 1966

ME Technical Report 036-1

September, 1966

Theoretical Study of Radiant Heat Exchange for Non-Gray Non-Diffuse Surfaces in a Space Environment

by

R. G. Hering

Research Grant No.
NASA NGR-14-005-036

FINAL REPORT

Department of Mechanical and Industrial Engineering
University of Illinois
Urbana, Illinois

Acknowledgment

This research was sponsored by the National Aeronautics and Space Administration under Grant NGR-14-005-036. This support under the direction of Mr. Conrad Mook of NASA is gratefully acknowledged.

The author expresses his gratitude to his principal assistants, Messrs. A. F. Houchens and T. F. Smith, both of whom have made significant contributions to this research effort. Mr. Houchens is continuing the theoretical study of real surface effects on radiant heat exchange. Further study of the bi-directional reflectance of engineering materials is being pursued by Mr. Smith. Thanks are also due to Mr. G. Hill who has given valuable assistance with the numerical calculations.

Foreword

The research summarized in this report was conducted during the last eighteen months with the financial support of the National Aeronautics and Space Administration under Research Grant No. NGR-14-005-036. The research is being continued with the financial support of Jet Propulsion Laboratory, California Institute of Technology under JPL Sub Contract 951661.

The majority of the research performed has been or is in the process of being reported in detail through References 1-4. These journal articles are available to interested readers; therefore, this final report will not attempt to repeat the results reported in these references. Instead, an attempt is made to summarize the results and contributions and give details only for extensions which were not reported in these references.

Table of Contents

Nomenclature

dA_p, dA_Q	differential areas at p & Q, respectively
a	correlation distance
a_0	geometry dimension
B(P)	radiosity at P
b_0	geometry dimension
C_i	coefficients for plate i as defined in Eqs. (4.2.8) and (4.2.9)
E(P)	emissive power at P
F_i	function defined in Eqs. (4.2.5) and (4.2.20)
$f_{n\gamma}(x_i,x_j)$	geometric function defined in Eq. (4.2.21)
$f(\psi,\pi;\theta,\vartheta)$	bi-directional reflectance of a perfectly conducting material for energy incident from (ψ,π) direction and reflected into (θ,ϑ) direction
G_i	coefficients for plate i as defined in Eqs. (4.2.8) and (4.2.9)
$H(x_i)$	irradiation of an element x_i
$I(P,\vec{r})$	radiant energy leaving P in $\vec{r}$ direction per unit time, solid angle, and area normal to $\vec{r}$ direction
K(P,Q)	geometric function ($\cos\theta_p \cos\vartheta_Q/\pi r^2_{pQ}$)
$K_\gamma(x_i,x_j)$	geometric function defined in Eqs. (4.2.4) and (4.2.19)
k	absorption index
L	length
N	number of elements
$\tilde{n}$	complex refractive index
n	refractive index
$\vec{n}_p,\vec{n}_Q$	outer surface normals to dA_p and dA_Q, respectively
q"(P)	net radiant energy transport to P per unit area and time

r_{PQ}	distance between P and Q
$\vec{r},\vec{s},\vec{i}$	direction vectors
R	directional reflectance as defined in Eq. (3.1.5)
$\bar{R}$	normalized bi-directional reflectance
$S(P,\vec{s})$	colliminated solar radiation illuminating P from $\vec{s}$ direction per unit time and irradiated area normal to direction of irradiation
T(P)	temperature at P
T_{ref}	reference temperature
$u_m(Z)$	unit step function; if $Z \geq 0$, $u = 1$; if $Z < 0$, $u = 0$
U	function defined after Eq. (3.1.3)
α	parameter defined by Eq. (3.2.3)
$\alpha(P,\vec{s})$	directional absorptance of surface P for energy incident in $\vec{s}$ direction
β	parameter defined by Eq. (3.2.3)
β_{ia},β_{ib}	dimensionless radiosities
δ	Dirac delta function
$\epsilon(P,\vec{s})$	directional emittance of surface P in $\vec{s}$ direction
$\epsilon(\theta)$	directional emissivity predicted by electromagnetic theory for a smooth, plane surface at angle θ from surface normal
γ	parameter defined by Eq. (3.2.3)
γ	opening angle
ξ	dimensionless distance
Φ	azimuthal angle of reflectance
ψ	polar angle of incidence
$\rho(P,\vec{r},\vec{s})$	bi-directional reflectance of surface P
$\rho(\theta)$	reflectivity predicted by electromagnetic theory for a smooth, plane surface irradiated at angle θ from surface normal

θ	polar angle of reflectance
θ_p, θ_Q	angles between line joining p and Q and the respective surface normals
θ_S	direction of solar field
σ	Stefan-Boltzmann constant
σ	rms height of roughness element
$d\omega$	element of solid angle

Subscripts

b	black
c	coherent
H	hemispherical
i	incident
i	radiation polarized parallel to plane of incidence
i,j	plate i and j, respectively
ic	incoherent
N	normal
s	radiation polarized perpendicular to plane of incidence
sp	specular
λ	monochromatic quantity

1.0 Introduction

This is the final report for NASA Research Grant NGR-14-005-036, "Theoretical Study of Radiant Heat Exchange for Non-Gray Non-Diffuse Surfaces in a Space Environment." This study was conceived as an examination of the influence of the spectral and directional radiation property dependencies of typical spacecraft structural materials on radiant heat exchange and equilibrium temperatures in a space environment.

The objectives of the study were fourfold. First, to accurately evaluate the radiant heat exchange and equilibrium temperatures for a representative system of surfaces in a space environment accounting for spectral and directional surface property characteristics. Results of such analysis can provide a standard of comparison for all currently employed simplified theories of radiant transfer and provide the basis for the development of improved methods. Secondly, to determine the accuracy of the gray completely diffuse and gray diffusely emitting-specularly reflecting theories of surface heat exchange for predicting heat transfer and equilibrium temperatures. Thirdly, to initiate the development of improved methods for radiant heat transfer analysis which can adequately account for the radiating character of engineering materials in an accurate, yet reasonably simple, manner. Finally, to provide the direction required for experimental radiation property measurement programs in order that the required property information is available to implement the improved theories for use by spacecraft thermal control designers.

A method of analysis for evaluating radiant heat transfer between non-gray non-diffuse surfaces is introduced first in Section 2.0. The remainder of the section is devoted to a description of the system and associated

environment selected for study and the relationship of the widely used gray theories of radiant transfer to the real surface analysis previously introduced. The detailed surface property information required for the non-diffuse, non-gray analysis is essentially embodied in the bi-directional reflectance of the participating surfaces. Two models for bi-directional reflectance of metal surfaces as well as directional and hemispherical surface radiation properties are reviewed in Section 3.0. Although heat transfer results are not yet available for the non-gray non-diffuse surface analysis, intensity distributions for a simplified version of the selected system are given and discussed in Section 4.1. Heat transfer and equilibrium temperatures predicted by gray theory are also presented in Section 4.0. These are intended to extend the scope of the results already available and thereby provide sufficient information to adequately evaluate the accuracy of gray theory. The results of the research effort and conclusions derived therefrom are summarized in Section 5.0.

Early in the research effort, a study of the bi-directional reflectance model originally proposed for use in the heat transfer analysis revealed that it displayed certain inadequacies. As a result of this finding, another model was studied and found superior in many respects. This unanticipated study of bi-directional reflectance has delayed the heat transfer study to the point where results from the non-gray non-diffuse analysis are not yet available.

2.0 Method of Analysis

The purpose of this section is threefold. First to present the method of analysis employed for the evaluation of radiant heat transfer and equilibrium surface temperatures accounting for the spectral dependence and non-diffuse character of radiation properties of engineering materials. Secondly, to focus attention on the information required to implement the analysis and, in particular, the system and associated environment chosen for study. Thirdly, to demonstrate that the widely used idealistic theories of radiant exchange analysis, namely the gray diffusely emitting-diffusely reflecting and gray diffusely emitting-specularly reflecting theories, are limiting forms of the non-gray non-diffuse analysis.

Certain simplifying assumptions are employed in the analysis. These are not expected to seriously impair the relevancy of the analysis to space applications. It is assumed that surface heat exchange occurs only by radiant energy transport and except for the presence of the solar field, other external sources of thermal radiation are negligible in comparison to the solar field and surface emission. The interacting surfaces are taken opaque and the intervening media diathermanous with unit refractive index. Only steady transport is considered and the influence of polarization on radiant exchange neglected. Figure 1 illustrates a typical two surface system in the presence of a collimated solar radiation field. This general system is used in the discussion to follow.

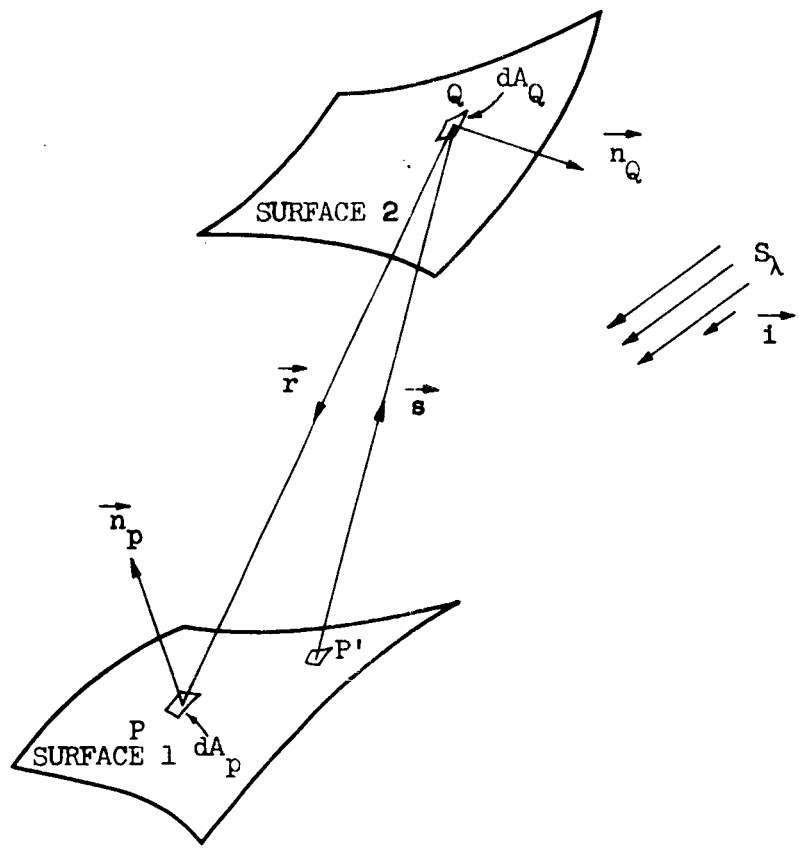

Fig. 1 Typical two surface system in a collimated solar field.

2.1 Non-Gray Non-Diffuse Surfaces

The local radiant heat flux to a typical element of a surface, say the elemental area dA_p located at point P of the surface designated 1 (See Fig. 1) may be evaluated as the difference between the absorbed irradiation and the emission.

$$q''(P)=\pi \int_0^\infty \int_{A_Q} \alpha_\lambda(P,\vec{r}) I_\lambda(Q,\vec{r}) K(P,Q) dA_Q d\lambda + \int_0^\infty \alpha_\lambda(P,\vec{i}) S_\lambda(P,\vec{i}) \cos(\vec{n}_p,-\vec{i}) d\lambda - \epsilon_H(P)\sigma T^4(P) \qquad (2.1.1)$$

The terms on the right-hand side of Eq. (2.1.1) represent in the order in which they appear; absorbed irradiation from all surfaces or portions of surfaces observed from P, directly incident solar radiation absorbed at P and the emission of dA_p. The contribution of solar irradiation appears in the local radiant heat loss expression only for those surface elements directly illuminated by the solar field. The symbols $\alpha_\lambda(P,\vec{r})$ and $\alpha_\lambda(P,\vec{i})$ represent the local monochromatic directional absorptance for irradiation incident from the $\vec{r}$ and $\vec{i}$ directions, respectively, whereas ϵ_H denotes the local hemispherical emittance. $K(P,Q)$ and $\cos(\vec{n}_p,-\vec{i})$ are geometrical parameters which may be evaluated after specification of the orientation of the surfaces and direction of the collimated solar field $S_\lambda(P,\vec{i})$. Thus, if the spectral properties of the surface ($\alpha_\lambda, \epsilon_\lambda$), spectral distribution and direction of the solar field ($S_\lambda(P,\vec{i})$), geometry of the system, and the temperature distribution (or radiant flux distribution) are specified, the local heat flux (or local temperature) may be evaluated provided the spectral radiant intensity I_λ is available.

The local spectral radiant intensity is determined from the following integral equation:

$$I_\lambda(Q,\vec{r}) = \epsilon_\lambda(Q,\vec{r})E_{b,\lambda}(Q) + \rho_\lambda(Q,\vec{i},\vec{r})\frac{}{\pi} S_\lambda(Q,\vec{i})\cos(\vec{n}_Q,-\vec{i}) +$$

$$\int_{A_{P'}} \rho_\lambda(Q,\vec{s},\vec{r})I_\lambda(P',\vec{s})K(P',Q)dA_{P'} \qquad (2.1.2)$$

where $\rho_\lambda(Q,\vec{s},\vec{r})$ is the bi-directional (or bi-angular) reflectance and $E_{b,\lambda}$ the local spectral emissive power of a black surface given by the Planck function. Equation (2.1.2) and an analagous equation for $I_\lambda(P',\vec{s})$ constitute a pair of simultaneous integral equations which require solution at each point on the surfaces for all possible directions in every wave length interval of importance. Once having determined such a solution for surfaces of specified temperature, the local radiant heat flux follows directly from Eq. (2.1.1). An iterative procedure involving both Eqs. (2.1.1) and (2.1.2) is necessary to determine the temperature distribution when the local flux is specified since the temperature enters both equations parametrically.

The system chosen for analysis is shown in Figure 2. It consists of two finite length plates with uniform properties and infinite in extent normal to the figure. This system was chosen because of its simple geometrical character, the availability of heat transfer results of previous investigators for certain limiting situations, and the important features of spacecraft heat transfer which are readily incorporated. Among the latter are interreflection phenomena and solar shading effects. Moreover, by appropriate selection of geometrical parameters, the results for this system find direct application to "radiant energy piping," portions of louver systems, radiation shields, cover glasses on solar collectors and other engineering systems. Having selected the geometry, the geometrical parameter K(P,Q)

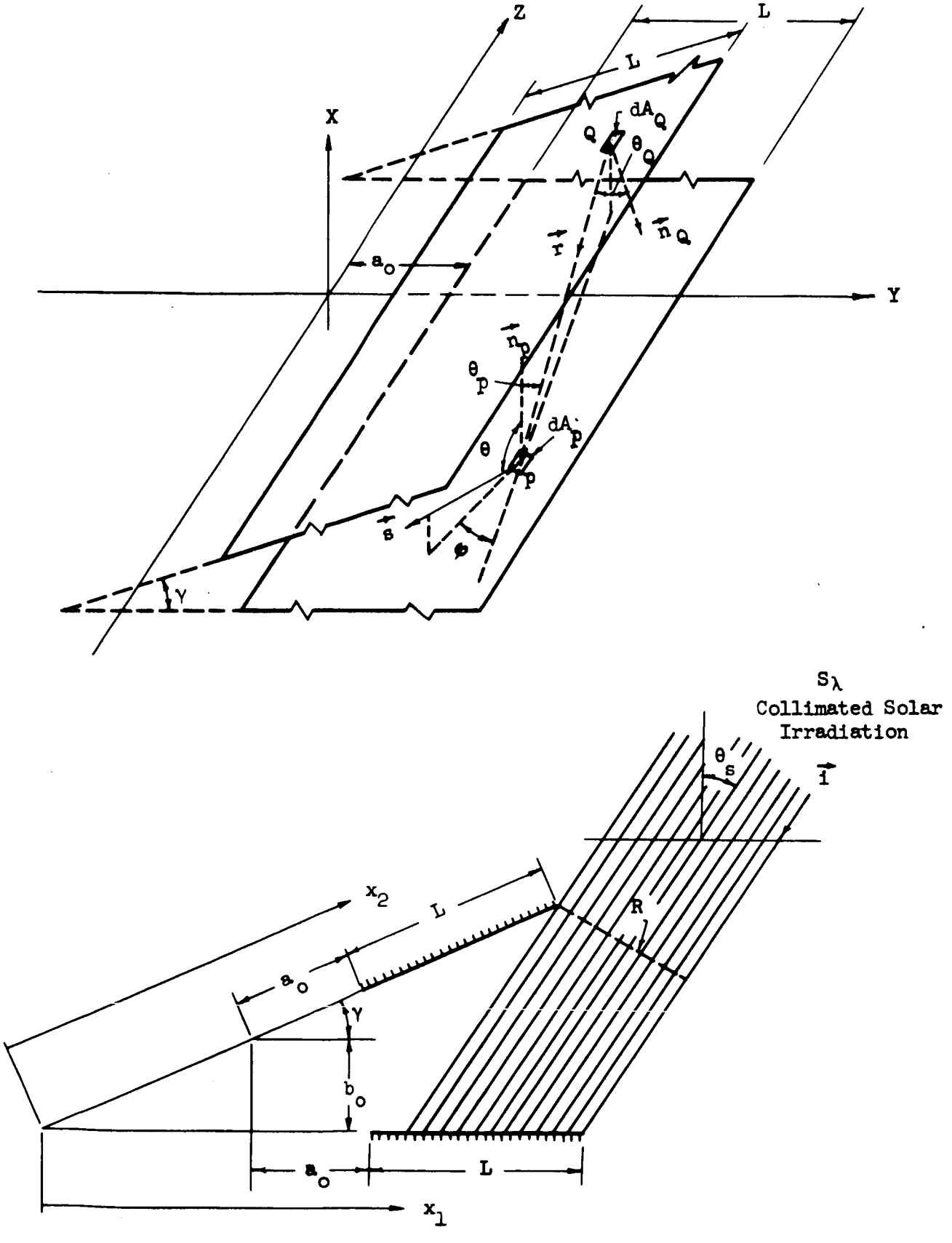

Fig. 2 Geometry of analysis.

entering Eqs. (2.1.1) and (2.1.2) is readily evaluated.

The only aspect of the system environment requiring further elucidation is the solar field. The solar field is taken collimated and in the plane of the figure with the direction ($\vec{i}$) left as a parameter in the analysis. Johnson's [5]* spectral distribution of the solar intensity is used. With the specification of the environment, the geometrical parameter $\cos(\vec{n}_p, -\vec{i})$ is defined in terms of the selected value for the direction of incidence and the local surface normal.

The thermal surface conditions initially chosen for investigation are those of uniform temperature and zero radiant heat loss. The latter provides so-called "equilibrium temperatures" which represent the maximum temperatures a system can attain for a specified external irradiation field in the absence of other modes of heat exchange. When the temperatures of the participating surfaces are specified interest lies in the evaluation of radiant heat transfer whereas for zero radiant heat loss, equilibrium temperatures are determined.

It remains to select the surface properties for the analysis. Section 3.0 is devoted to a discussion of two models for bi-directional reflectance and also directional radiation properties. Before passing on to these topics, the simplifications realized in the analysis by the commonly employed assumptions of spectral independence of properties (gray surfaces) and of diffusely reflecting or specularly reflecting surfaces are considered in the following sections. Some results obtained using these idealistic theories are given later.

*Numbers in brackets [ ] designate references in Section 6.0.

2.2 Gray Surfaces

Most reported radiant heat exchange analyses employ the gray assumption, that is, the spectral dependence of radiation properties is ignored. Although no such surfaces exist, the results obtained often provide considerable insight into the radiant exchange processes as well as sufficiently accurate results to warrent their uses in predicting general trends.

Introducing the assumption that all participating surfaces are gray yields the following equalities between total and spectral property values:

$$\epsilon_{H,\lambda} = \epsilon_H, \quad \alpha_\lambda = \alpha, \quad \rho_\lambda = \rho, \quad \epsilon_\lambda = \epsilon \tag{2.2.1}$$

Also denoting the spectrum integrated energy quantities with the symbolism

$$I = \int_0^\infty I_\lambda d\lambda, \quad S = \int_0^\infty S_\lambda d\lambda, \quad E_b = \int_0^\infty E_{b,\lambda}\, d\lambda = \sigma T^4 \tag{2.2.2}$$

the equations for local radiant flux and intensity transform to:

$$q''(P) = \pi \int_{A_Q} \alpha(P,\vec{r})\, I(Q,\vec{r})\, K(P,Q) dA_Q + \alpha(P,\vec{i})\, S(P,\vec{i})\, \cos(\vec{n}_p, -\vec{I}) - \epsilon_H(P)\, \sigma T^4(P) \tag{2.2.3}$$

$$I(Q,\vec{r}) = \epsilon(Q,\vec{r})\, \frac{\sigma T^4(Q)}{\pi} + \rho(Q,\vec{i},\vec{r})\, \frac{S(Q,\vec{I})}{\pi} \cos(\vec{n}_Q, -\vec{i}) + \int_{A_{P'}} \rho(Q,\vec{s},\vec{r})\, I(P',\vec{s})\, K(P',Q) dA_{P'} \tag{2.2.4}$$

The simplification introduced by this assumption is evident. No longer is it necessary to solve the integral equations for intensity at each wave length. This, of course, greatly reduces the numerical effort normally required to evaluate results from radiant exchange analysis.

2.2.1 Diffusely Emitting--Diffusely Reflecting Surfaces

One of the commonly employed idealizations for the directional variation of surface emission and reflection is that corresponding to a diffuse surface. A diffuse surface emits energy and reflects incident energy with equal intensity in all directions. Therefore, the directional emittance is equal to the hemispherical emittance. Although the directional reflectance of a diffuse surface need not be identical for all directions of incident energy, it usually is so taken and this further stipulation is employed here. For a diffuse surface, the bi-directional reflectance, directional reflectance and hemispherical reflectance are equal. The heat flux and intensity relations corresponding to gray diffusely emitting-diffusely reflecting surfaces are as follows:

$$q''(P) = \pi \int_{A_Q} \alpha_H(P) I(Q) K(P,Q) dA_Q + \alpha_H(P) S(P,\vec{i}) \cos(\vec{n}_p, -\vec{i}) - \epsilon_H(P) \sigma T^4(P) \qquad (2.2.5)$$

$$I(Q) = \epsilon_H(Q) \frac{\sigma T^4(Q)}{\pi} + \rho_H(Q) \frac{S}{\pi}(Q,\vec{i}) \cos(\vec{n}_Q, -\vec{i}) + \int_{A_{P'}} \rho_H(Q) I(P') K(P',Q) dA_{P'} \qquad (2.2.6)$$

The further simplication introduced by the additional assumption of a diffuse surface eliminates the need to evaluate the intensity in different directions. It is customary in diffuse analysis to employ the concept of radiosity, $B(Q)$. Radiosity is simply the total energy leaving a surface element per unit time and area and is related to the intensity of a diffuse surface by the relation

$$B = \pi I.$$

Introducing radiosity into Eqs. (2.2.5) and (2.2.6) yields the following equations:

$$q''(P) = \int_{A_Q} \alpha_H(P)B(Q)K(P,Q)dA_Q + \alpha_H(P)S(P,\vec{i})\cos(\vec{n}_p,-\vec{i}) - \varepsilon_H(P)\sigma T^4(P) \qquad (2.2.7)$$

$$B(Q) = \varepsilon_H(Q)\sigma T^4(Q) + \rho_H(Q)S(Q,\vec{i})\cos(\vec{n}_Q,-\vec{i}) + \int_{A_{P'}} \rho_H(Q)B(P')K(P',Q)dA_{P'} \qquad (2.2.8)$$

The determination of the solution to Eq. (2.2.8) for various geometrical arrangements of different systems of surfaces has been the goal of many previous investigators.

2.2.2 Diffusely Emitting--Specularly Reflecting Surfaces

A second model for surface reflection which has received considerable attention in the recent literature is that of specular reflection. In a specular reflection, the incident beam leaves the surface in the plane of incidence with the polar angle relative to the surface normal equal to that of the incident beam. Also, the solid angles of transfer for incident and reflected radiation are equal. Diffuse and specular reflection are usually considered as the two limiting cases for reflection from a surface. Except for a recently reported analysis [3], the dependence of the reflectance magnitude on the direction of incidence is usually ignored and the diffuse emission model retained. This serves to significantly reduce the complexity of specular reflection analysis.

The bi-directional reflectance of a specularly reflecting surface is a Dirac delta function in which case the integral in the intensity relation of Eq. (2.2.4) degenerates to the single term $\rho_H(Q)I(P',\vec{r}_{sp})$ where $\vec{r}_{sp}$ denotes the direction of the incident ray which is specularly reflected into the $\vec{r}$ direction. Then for a gray diffusely emitting-specularly reflecting

surface, the heat flux and intensity expressions become:

$$q''(P) = \pi \int_{A_Q} \alpha_H(P) I(Q,\vec{r}) K(P,Q) dA_Q + \alpha_H(P) S(P,\vec{i}) \cos(\vec{n}_p, -\vec{i})$$

$$- \epsilon_H(P)\, \sigma T^4(P) \qquad (2.2.9)$$

$$I(Q,\vec{r}) = \frac{\epsilon_H(Q)\, \sigma T^4(Q)}{\pi} + \rho_H(Q) I(P', \vec{r}_{sp})$$

$$+ \rho_H \frac{(Q)\ S(Q,\vec{i}) \cos(\vec{n}_Q, -\vec{i})}{\pi} \qquad (2.2.10)$$

The last term in the intensity relation is retained only for the direction corresponding to $\vec{r}_{sp}$. Equation (2.2.10) has in principle been solved by a number of investigators employing the concepts of ray tracing or image surfaces.

3.0 Radiation Properties

Implementation of the heat transfer analysis requires surface radiation property information, particularly an acceptable description for the bi-directional reflectance of engineering materials. Two models for the bi-directional reflectance are considered in Section 3.1. As a result of this study, the Davies model [6] originally proposed for the heat transfer study was discarded in favor of the Beckmann model [7]. Directional and hemispherical properties are considered in Sections 3.2 and 3.3 respectively. Unlike previous investigations, the purpose of these studies was to evaluate the accuracy of certain approximate formulas for calculating directional and hemispherical properties. The relative simplicity of the approximate relations is particularly attractive as a means of reducing the complexity and calculation time required in the already difficult and time consuming heat transfer calculations. Criteria are developed which assure a prescribed accuracy in the evaluation of directional and hemispherical properties when using the simpler approximate relations.

3.1 Bi-Directional Reflectance

A number of models for the reflection of electromagnetic radiation from surfaces with widely different topography have been proposed in the literature [7]. Most of these are derived for electrical conductors of infinite conductivity. The limitation to infinite conductivity eliminates the need to consider volume effects since under such conditions the reflection process is a surface phenomenon. This artifice greatly simplifies the analysis but, of course, places severe limitations on the models. The infinite conductivity results are usually modified in some approximate manner for application to engineering materials.

The two models examined here consider only the influence of surface roughness on the distribution of reflected energy. Since details of this study are reported in reference [1], discussion is limited to the more significant results and their implications for the heat transfer study.

The influence of surface roughness on the radiation properties of materials may be generally discussed in terms of the magnitude of the optical roughness of the surface. By optical roughness, reference is made to the ratio of a characteristic dimension of the surface asperity height to a characteristic wave length of the incident radiation. For optical roughness values much greater than unity, multiple reflections occur between roughness elements resulting in increased emittance and decreased reflectance as compared to that of the same material with an optically smooth surface. This, of course, is the phenomenon which results in the so-called "cavity effect" whereby the apparent emittance or absorptance of a cavity is larger than that of the constituent material. For large optical roughness, the methods of geometrical optics apply and results using such analysis have been reported for simple cavity shapes. On the other hand when optical roughness is small, the influence of multiple reflections is small and the emittance and reflectance of the surface are essentially identical to those of an optically smooth surface. However, the distribution of reflected energy is strongly affected by the surface roughness. For small optical roughness values, the distribution of reflected radiation may be described in terms of a diffraction model.

The range of optical roughness for spacecraft structural materials is of interest in establishing the type of model more appropriate in the present study. For metals, surface roughnesses characteristic of those

produced by normal machining, grinding, and polishing operations result in mechanical root mean square roughness heights of about one micron with a half or fourth probably more representative. For surfaces of these roughnesses and radiation in the infrared (0.8-100 μ) the approximate range of optical roughness is 0.003 to 1.0. This range of optical roughness also appears appropriate for solar radiation at least for the smaller mechanical roughness of polished surfaces. In view of the range of optical roughness values of interest, a diffraction model appears appropriate for describing the influence of surface roughness on the radiation properties of metals. Two such models, namely those of Beckmann [7] and Davies [6] are here discussed.

Both the Davies and Beckmann bi-directional reflectance models consider the reflection of unpolarized radiation from a perfectly conducting material with random surface heights distributed according to the Gaussian distribution with standard deviation σ. The two dimensional distribution function is Gaussian with auto-correlation coefficient also Gaussian with correlation distance a. Physically, σ represents the root mean square surface roughness height and a is proportional to the reciprocal of the root mean square slope of the surface roughness profile. Interreflections and shadowing affects are neglected and analysis limited to ratios of correlation distance a to wave length λ much larger than unity ($a/\lambda \gg 1$). Davies, however, treats only the limiting cases of very small ($\sigma/\lambda \ll 1$) and very large ($\sigma/\lambda \gg 1$) optical roughness. Beckmann [7] points out that Davies initial point of departure in his analysis limits the results to surfaces with extremely small roughness profile slopes and therefore the Davies' result for very large optical roughness values is particularly questionable.

The results of both analyses for bi-directional reflectance of infinite conductivity materials, $f_\lambda(\psi,\pi;\theta,\Phi)$,* are conveniently expressed as the sum of two terms. One term, $f_{\lambda,c}(\psi)$, represents the coherently reflected energy and the other, $f_{\lambda,ic}(\psi,\pi;\theta,\Phi)$, denotes the incoherently reflected energy. Beckmann's analysis yeilds

$$f_\lambda(\psi,\pi;\theta,\Phi) = f_{\lambda,c}(\psi)\, U(u) + f_{\lambda,ic}(\psi,\pi;\theta,\Phi) \qquad (3.1.1)$$

where

$$f_{\lambda,c}(\psi) = \frac{\pi}{\cos\psi d\omega_i} \exp\left\{-\left[4\pi\left(\frac{\sigma}{\lambda}\right)\cos\psi\right]^2\right\} \qquad (3.1.2)$$

$$f_{\lambda,ic}(\psi,\pi;\theta,\Phi) = \frac{\pi^2(\frac{a}{\lambda})^2}{\cos\theta\cos\psi}\left[\frac{1+\cos\theta\cos\psi-\sin\theta\sin\psi\cos\Phi}{\cos\theta+\cos\psi}\right]^2 \cdot$$

$$\exp\left\{-\left[2\pi\left(\frac{\sigma}{\lambda}\right)(\cos\theta+\cos\psi)\right]^2\right\}\cdot\sum_{m=1}^{\infty}\frac{\left[4\pi^2(\frac{\sigma}{\lambda})^2(\cos\theta+\cos\psi)^2\right]^m}{m\cdot m!}\cdot$$

$$\exp\left\{-\frac{\pi^2}{m}\left(\frac{a}{\lambda}\right)^2\left[\sin^2\psi+\sin^2\theta-2\sin\psi\sin\theta\cos\Phi\right]\right\} \qquad (3.1.3)$$

$$U = u(\theta-\psi)u(\psi+d\psi-\theta)u(\Phi)u(d\Phi-\Phi)$$

with u(z) the unit step function which has the value 0 for argument less than zero and 1 otherwise. The Davies model for small optical roughness differs only in the expression for the incoherently reflected energy. For the Davies model, Equation (3.1.3) is replaced with the following expression.

$$f_{\lambda,ic}(\psi,\pi;\theta,\Phi) = \pi^4\left(\frac{a}{\lambda}\right)^2\left(\frac{\sigma}{\lambda}\right)^2\frac{(\cos\theta+\cos\psi)^4}{\cos\theta\cos\psi}\cdot$$

$$\exp\left\{-\pi^2\left(\frac{a}{\lambda}\right)^2\left[\sin^2\psi+\sin^2\theta-2\sin\psi\sin\theta\sin\Phi\right]\right\} \qquad (3.1.4)$$

The angles in the previous expressions are shown in Fig. 3.

---

*In Figures 3, 4, and 5, $\phi = \Phi$.

Both models satisfy the Helmholtz reciprocity requirement and predict that the distribution of coherently reflected energy depends only on the angle of incidence, solid angle containing the incident energy and the single surface parameter optical roughness, (σ/λ). Figure 4 illustrates the results obtained for the coherent component of both models as a function of the optical roughness of the surface for a range of angles of incidence. The trends are as expected. For specified angles of incidence the coherently reflected energy leaving the surface in the specular direction diminishes with increasing optical roughness and the surface appears optically smoother with increasing angles of incidence for a specified optical roughness. Experiment [8] appears to confirm the coherent term.

The incoherent term of the bi-directional reflectance models contributes to the energy reflected into the specular direction as well as all other possible directions. According to both models the distribution of incoherently reflected energy depends on <u>two</u> surface roughness parameters (σ/λ) and (a/λ). The dependence on the root mean square slope of surface roughness does not appear to have been fully recognized by other investigators although experimental evidence appears to substantiate this dependence [8]. Figure 5 illustrates results obtained from the Beckmann model for a range of optical roughness values with an angle of incidence of 10°. The distributions obtained for three values of (a/λ) are shown for each value of (σ/λ). Of particular significance is the increasing specularity of the surface with increasing (a/λ) for a selected (σ/λ) value. That is, the model predicts that a surface of specified optical roughness approaches a specularly reflecting surface as the roughness slopes diminish. Due to inadequate description of surface roughness, specifically values for (a/λ), the only data apparently available

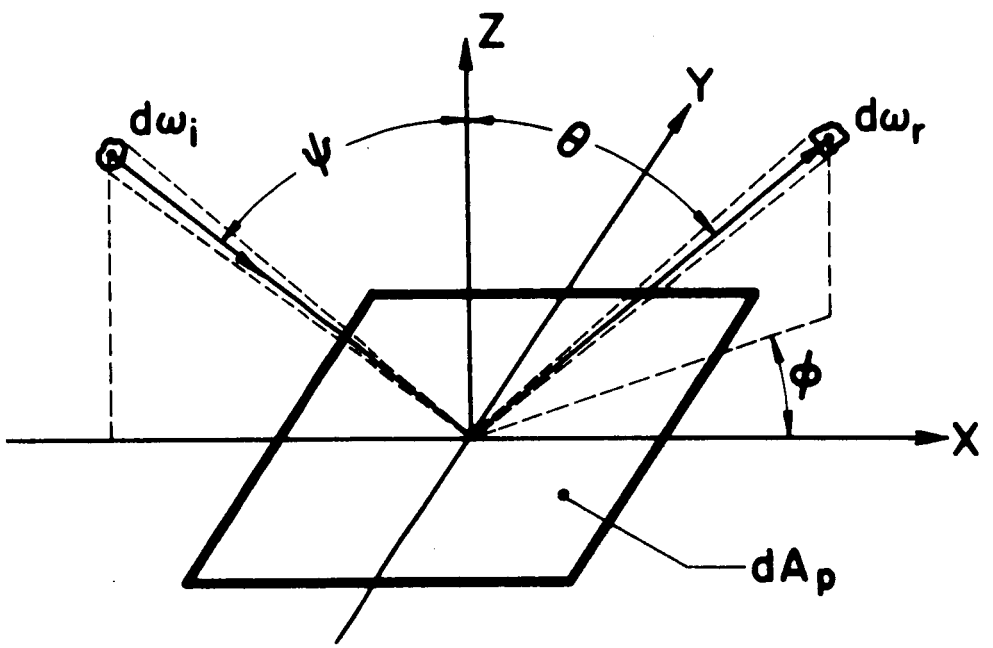

Fig. 3 Angles of incidence and reflection.

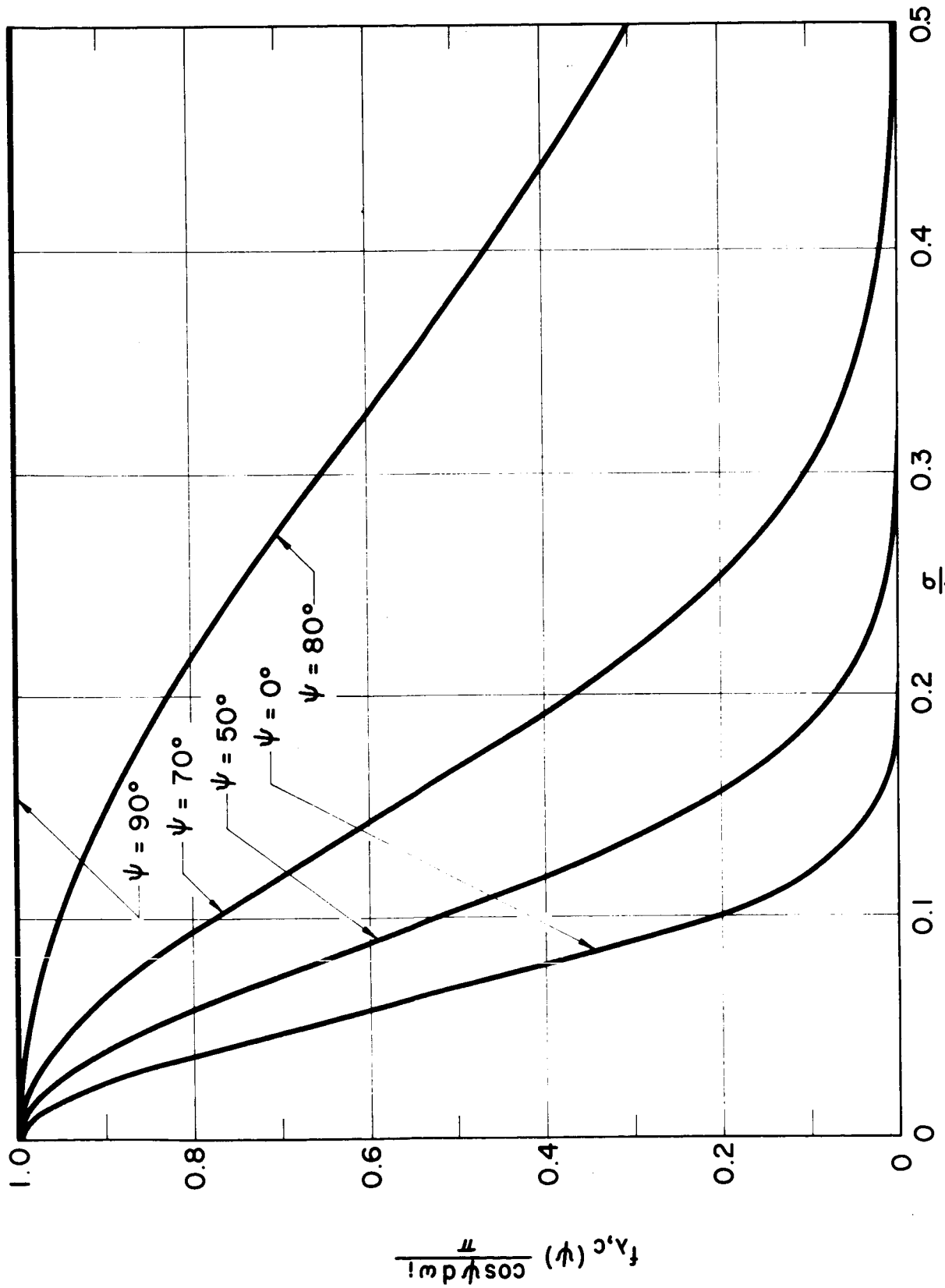

Fig. 4 Coherence reflectance from Beckmann's model.

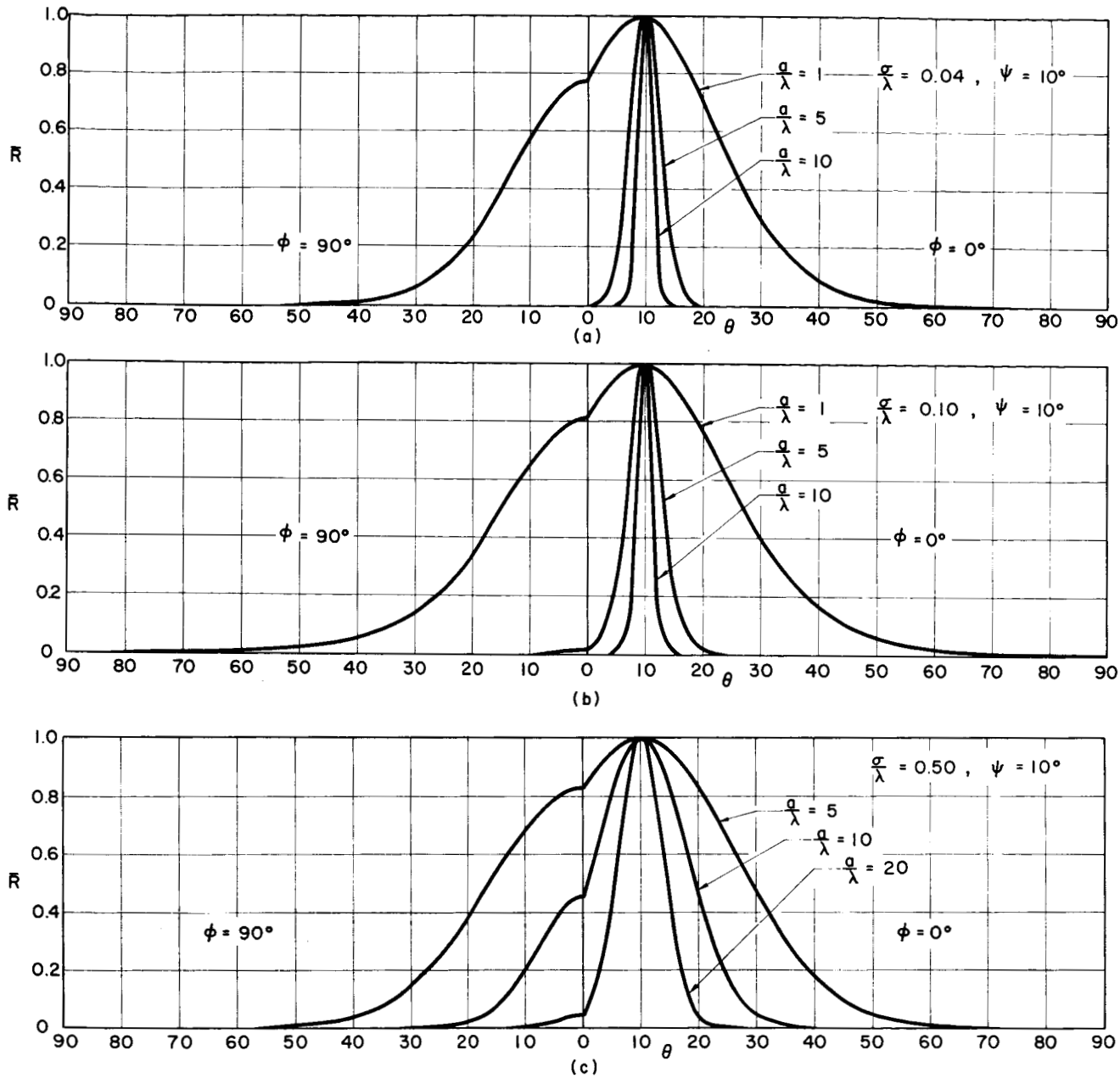

Fig. 5 Normalized incoherent bi-directional reflectance from Beckmann's model.

$$\bar{R} \equiv f_{\lambda,ic}(\psi,\pi;\theta,\Phi) \cos\theta / f_{\lambda,ic}(\psi,\pi;\psi,0) \cos\psi$$

to evaluate the Beckmann model is that of Birkebak [8]. Although this data is inadequate to verify the model, a typical comparison is shown in Figure 6. Further details and comparisons are available in reference [1].

Since both models are derived for perfectly conducting materials, all incident energy should be accounted for in the reflected beam, that is, the directional reflectance should be unity independent of angle of incidence and the surface roughness parameters (σ/λ) and (a/λ). The directional reflectance is determined by multiplying the bi-directional reflectance with $(\cos\theta\, d\omega_r/\pi)$ and integrating over all solid angles.

$$R_\lambda = \frac{1}{\pi}\int_0^{2\pi}\int_0^{\pi/2} f_\lambda \cos\theta \sin\theta \, d\theta \, d\varphi \qquad (3.1.5)$$

Results obtained for the directional reflectance R_λ are given in Table I for the Beckmann and Davies models. It is evident from these results that unit directional reflectance is generally not obtained. The Beckmann model, however, satisfies this requirement quite well and is notably superior to that of Davies. The Davies model predicts unit directional reflectance only in the range of surface roughness parameter values in which the departure from purely specular reflection is so slight as to be neglected with little loss in accuracy. Since the unit reflectance criterion is essentially an energy conservation requirement, it is clear that the use of the Davies model, which grossly violates energy conservation in the range of optical roughness parameters of interest, could render heat exchange results useless. It was this finding early in the research effort which prompted the study of the Beckmann bi-directional reflectance model.

As noted earlier, the bi-directional reflectance models discussed were derived for perfectly conducting materials and must be modified for use with

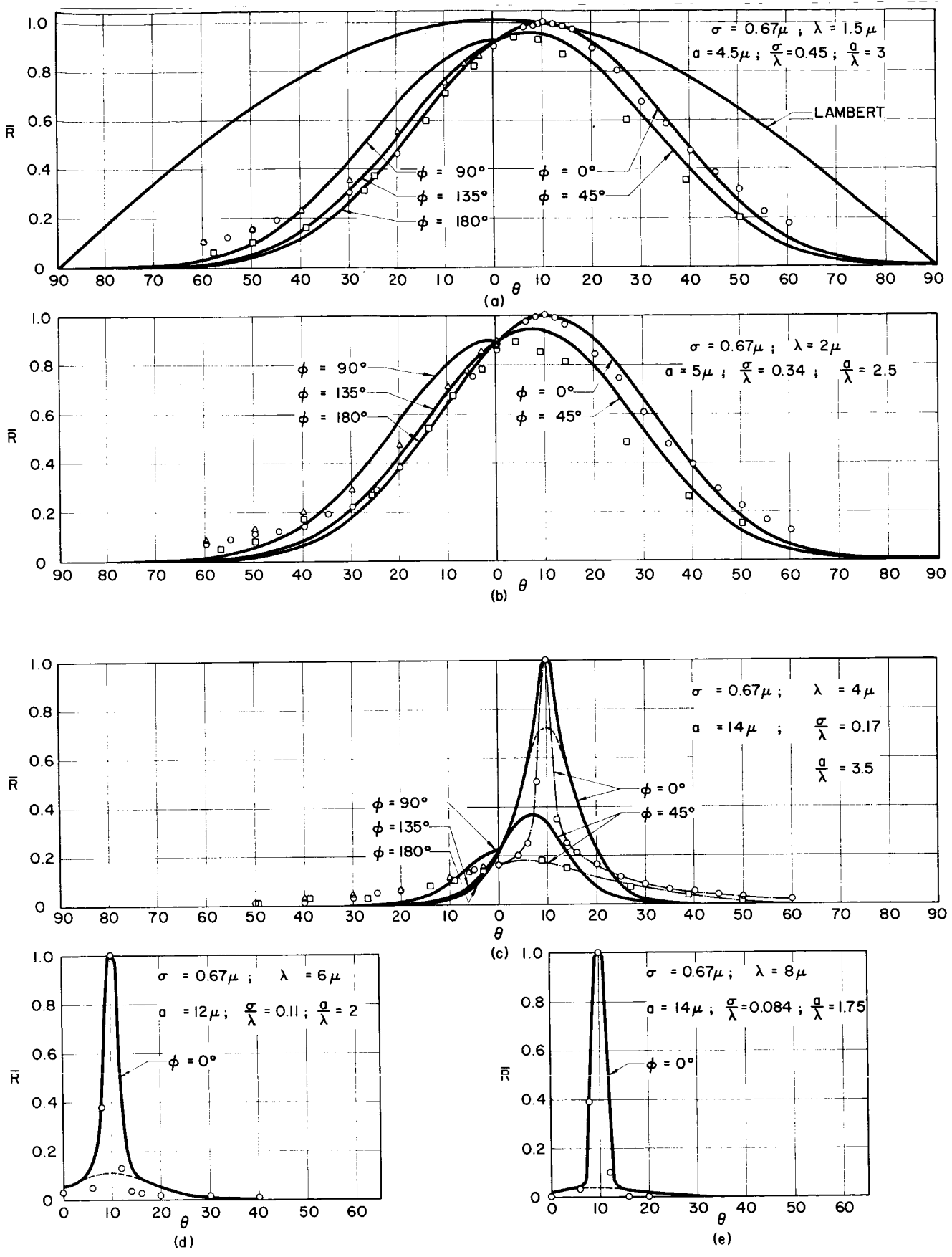

——— Sum of coherent and incoherent components.
– – – – Incoherent component.
—·— Curve connecting data.

Fig. 6 Comparison of Beckmann's model with Birkebak's data.
(Data for ground glass Al. coated; ref. [8]; $\sigma = 0.67\mu$; $\psi = 10^{\circ}$)
$\bar{R} = f_{\lambda}(\psi,\pi;\theta,\phi)\cos\theta / f_{\lambda}(\psi,\pi;\psi,0)\cos\psi$

TABLE 1

Directional Reflectance from Beckmann's Model and Davies' Model*

$\frac{\sigma}{\lambda} = 0.01$					
	a/λ				
ψ	1.	5.	10.	50.	100.
0°	1.000 0.999	1.000 1.000	1.000 1.000	1.000 1.000	1.000 1.000
40°	0.998 0.999	1.000 1.000	1.000 1.000	1.000 1.000	1.000 1.000
80°	1.002 1.000	1.000 1.000	1.000 1.000	1.000 1.000	1.000 1.000

$\frac{\sigma}{\lambda} = 0.04$					
	a/λ				
ψ	1.	5.	10.	100.	
0°	1.000 1.017	1.000 1.029	1.000 1.029	1.000 1.029	
40°	0.9960 0.995	1.000 1.010	1.000 1.010	1.000 1.011	
80°	1.025 1.015	1.002 1.001	0.999 1.000	0.999 1.000	

$\frac{\sigma}{\lambda} = 0.10$					
	a/λ				
ψ	1.	5.	10.	50.	100.
0°	1.001 1.705	1.000 1.782	1.000 1.785	1.000 1.785	1.000 1.785
40°	0.981 1.226	1.000 1.319	1.000 1.322	1.000	1.000 1.325
80°	1.149 1.094	1.009 1.009	0.999 1.000	1.000 1.001	1.000 1.001

*Values above and below dashed line refer to Beckmann's model and Davies' model, respectively

TABLE 1 continued

$\frac{\sigma}{\lambda} = 0.16$					
	a/λ				
ψ	1.	5.	10.	50.	100.
0°	0.996 / 3.855	1.000 / 4.052	1.000 / 4.058	1.000 / 4.600	1.000 / 4.600
40°	0.961 / 2.218	1.000 / 2.457	1.000 / 2.464	1.000 / 2.466	1.000 / 2.466
80°	1.356 / 1.245	1.023 / 1.027	0.999 / 1.005	1.000 / 1.007	1.000 / 1.007

$\frac{\sigma}{\lambda} = 0.20$					
	a/λ				
ψ	1.	5.	10.	50.	100.
0°	0.985 / 5.999	1.000 / 6.306	1.000 / 6.315	1.000 / 6.318	1.000 / 6.318
40°		1.000 / 3.719	1.000 / 3.728	1.000 / 3.731	1.000 / 3.731
80°	1.518 / 1.389	1.034 / 1.048	0.998 / 1.013	1.000 / 1.017	1.000 / 1.017

$\frac{\sigma}{\lambda} = 0.50$					
	a/λ				
ψ	10	20	100	150	
0°	1.000 / 39.46	1.000 / 39.47	1.000 / 39.48	1.000 / 39.48	
40°	1.000 / 23.15	1.000 / 23.16	1.000 / 23.17	1.000 / 23.17	
80°	.981 / 1.470	.980 / 1.462	1.000 / 1.494	1.000 / 1.494	

engineering materials. One suggestion put forth is to simply multiply the bi-directional reflectance for infinite conductivity by the directional reflectance of finite conductivity materials with an optically smooth surface. Although this method is not completely satisfactory and other approximations are possible [1], it, as well as the general need to consider directional property dependencies, lead to a study of directional reflectance. The results of this study are discussed in Section 3.2.

As a result of this study of bi-directional reflectance, the Davies model was discarded and the heat exchange calculations based on that proposed by Beckmann. This was justified on the basis of two criteria. First, the development of the Beckmann model indicated a firmer theoretical foundation and a wider range of applicability in terms of the optical roughness parameters (σ/λ) and (a/λ). Secondly, the gross violation of the energy conservation requirement by the Davies model for optical roughness parameter values of interest in this investigation. This latter deficiency could render the results of the heat transfer study useless. Unfortunately, sufficient experimental data is not available to substantiate the Beckmann or, for that matter, any other model for bi-directional reflectance. However, qualitative agreement appears to exist with the limited data available although quantitative agreement is only fair.

3.2 Directional Properties

The directional radiation properties of optically smooth surfaces have been considered by many previous investigators. However, the intent of this study differs substantially from previous efforts in that the prime purpose is to ascertain the degree of validity of simplified formulae for directional properties. The exact relations of electromagnetic theory are particularly tedious to use in numerical calculations and the use of approximate relations can significantly reduce the complexity of the heat transfer calculations.

Electromagnetic theory provides directional reflectivity relationships for optically smooth uncontaminated surfaces in terms of the refractive and absorption indices of the material. The expressions for the specular reflectivity of a non-magnetic material are:

RADIATION POLARIZED PERPENDICULAR TO PLANE OF INCIDENCE ($\rho_{s,\lambda}$)

$$\rho_{s,\lambda}(\theta) = \frac{\cos^2\theta - 2n\alpha\cos\theta + n^2(1+k^2)\beta}{\cos^2\theta + 2n\alpha\cos\theta + n^2(1+k^2)\beta} \qquad (3.2.1)$$

RADIATION POLARIZED PARALLEL TO PLANE OF INCIDENCE ($\rho_{i,\lambda}$)

$$\rho_{i,\lambda}(\theta) = \frac{n^2(1+k^2)\cos^2\theta - 2n\gamma\cos\theta + \beta}{n^2(1+k^2)\cos^2\theta + 2n\gamma\cos\theta + \beta} \qquad (3.2.2)$$

with

$$\alpha^2 = \frac{(1+k^2)}{2}\left[\left(\frac{1-k^2}{1+k^2}\right) + \beta - \left(\frac{\sin^2\theta}{n^2(1+k^2)}\right)\right]$$

$$\beta^2 = \left[1 + \left(\frac{\sin^2\theta}{n^2(1+k^2)}\right)\right]^2 - \frac{4}{(1+k^2)}\left[\frac{\sin^2\theta}{n^2(1+k^2)}\right] \qquad (3.2.3)$$

$$\gamma = \frac{(1-k^2)}{(1+k^2)}\alpha + \frac{2k}{(1+k^2)}\sqrt{(1+k^2)\beta - \alpha^2}$$

where the optical constants n and k specify the real and imaginary components of the complex index of refraction

$$\tilde{n} = n(1 - ik) \tag{3.2.4}$$

and θ denotes the polar angle of the incident beam measured relative to the surface normal. The Fresnel reflectivity relations of Eqs.(3.2.1) and (3.2.2) are in essence spectral values since both n and k are strong functions of wave length. Also, these relations are strictly applicable when the medium adjacent to the reflecting surface is a vacuum or gas for which the refractive index is unity and absorption index zero. If the incident radiation is unpolarized, the monochromatic specular reflectance is the arithmetic mean of $\rho_{s,\lambda}$ and $\rho_{i,\lambda}$. Then

$$\rho_\lambda(\theta) = \frac{1}{2}(\rho_{s,\lambda} + \rho_{i,\lambda}) \tag{3.2.5}$$

where $\rho_\lambda(\theta)$ denotes the directional reflectivity for unpolarized radiation.

The complicated character of the exact reflectivity relations has inspired the use of simpler approximate formulae. The approximate relations considered here are those derived for the case where

$$n^2(1 + k^2) >> 1$$

When the above holds the factors α, β, and γ of Eq. (3.2.3) are approximately unity resulting in the following simpler expressions:

RADIATION POLARIZED PERPENDICULAR TO PLANE OF INCIDENCE ($\rho_{s,\lambda}$)

$$\rho_{s,\lambda}(\theta) = \frac{(n - \cos\theta)^2 + n^2k^2}{(n + \cos\theta)^2 + n^2k^2} \tag{3.2.6}$$

RADIATION POLARIZED PARALLEL TO PLANE OF INCIDENCE ($\rho_{i,\lambda}$)

$$\rho_{i,\lambda}(\theta) = \frac{(n - \frac{1}{\cos\theta})^2 + n^2k^2}{(n + \frac{1}{\cos\theta})^2 + n^2k^2} \qquad (3.2.7)$$

Either set of relations for reflectivity may be utilized for the directional absorptivity of opaque materials through the relation

$$\alpha_\lambda(\theta) = 1 - \rho_\lambda(\theta) \qquad (3.2.8)$$

and consequently, according to Kirchhoff's law,

$$\epsilon_\lambda(\theta) = \alpha_\lambda(\theta) \qquad (3.2.9)$$

for the directional emissivity as well. Representative results for the angular dependence of the components of the directional reflectivity ($\rho_{s,\lambda}$, $\rho_{i,\lambda}$) and the directional reflectivity for unpolarized radiation (ρ_λ) are illustrated in Figs. 7, 8, and 9 for values of the absorption index of 0.0, 0.5, and 4.0, respectively. The results for both the exact and approximate relations are shown in each figure for selected values of the refractive index. In general, the approximate relations give exceptionally accurate results especially for values of the absorption index exceeding 4.0. However, as might be expected, the directional reflectivity predicted for nonconductors ($k = 0.0$) for unit refractive index is in gross error. It is also evident from the figures that the approximate relations yield results of considerably greater accuracy for $\rho_{s,\lambda}(\theta)$ and $\rho_\lambda(\theta)$ than for $\rho_{i,\lambda}(\theta)$.

Criteria have been developed to assure a selected percentage accuracy by the use of the approximate relations. These are given in terms of the parameter $n^2(1 + k^2)$ for 1.0, 5.0, and 10.0 per cent accuracy in Table 2. The use of this table may be illustrated by the following example. If the

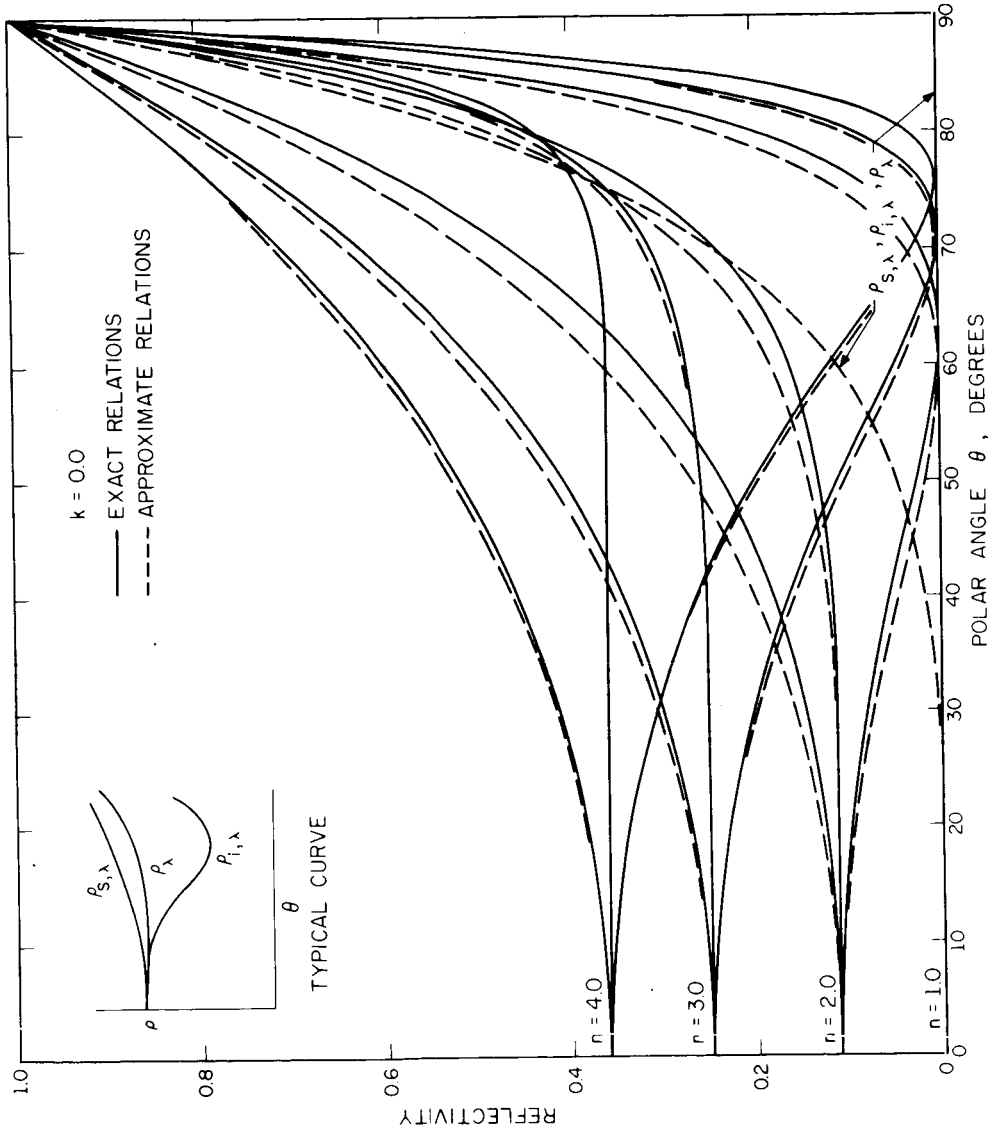

Fig. 7 Directional reflectivity for selected values of n (k = 0.0).

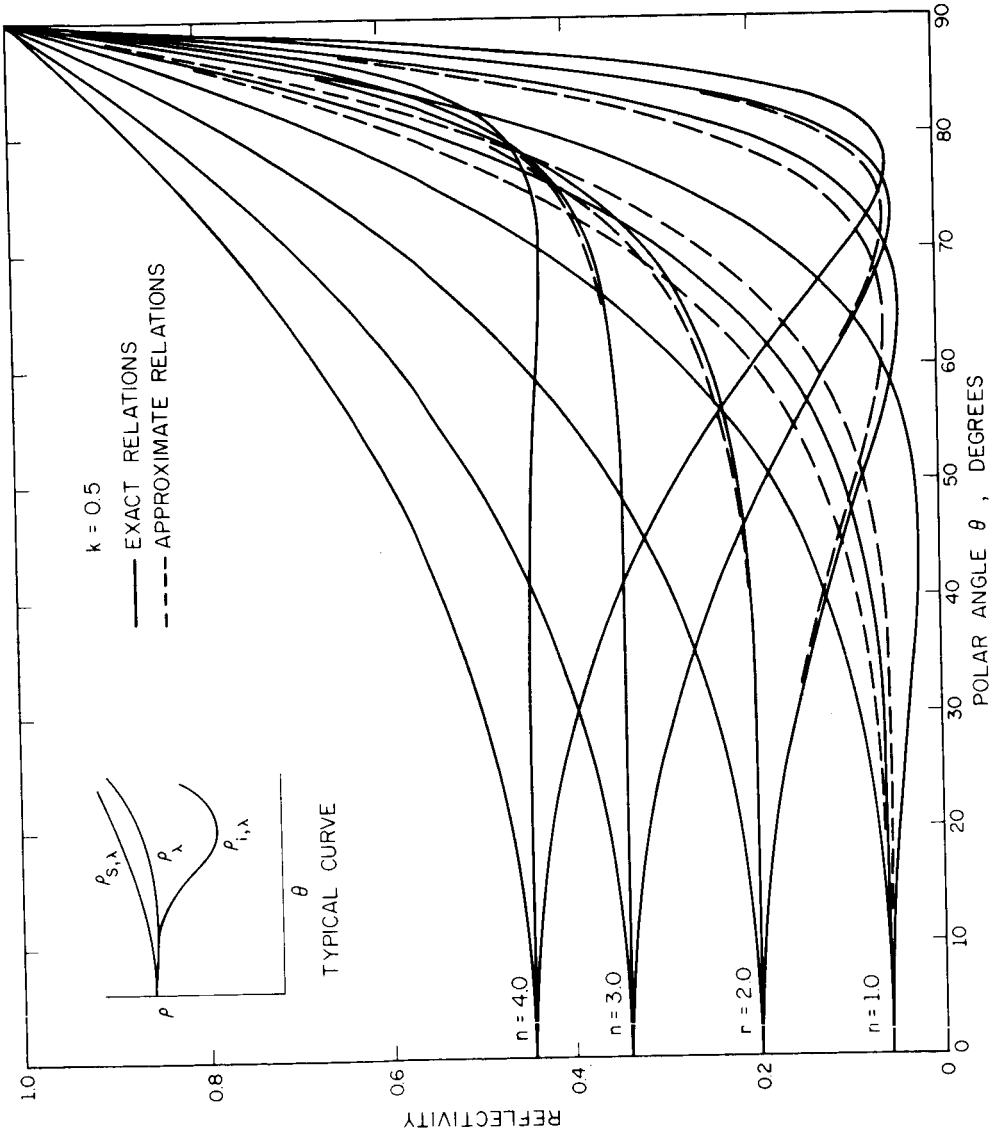

Fig. 8 Directional reflectivity for selected values of n (k = 0.5).

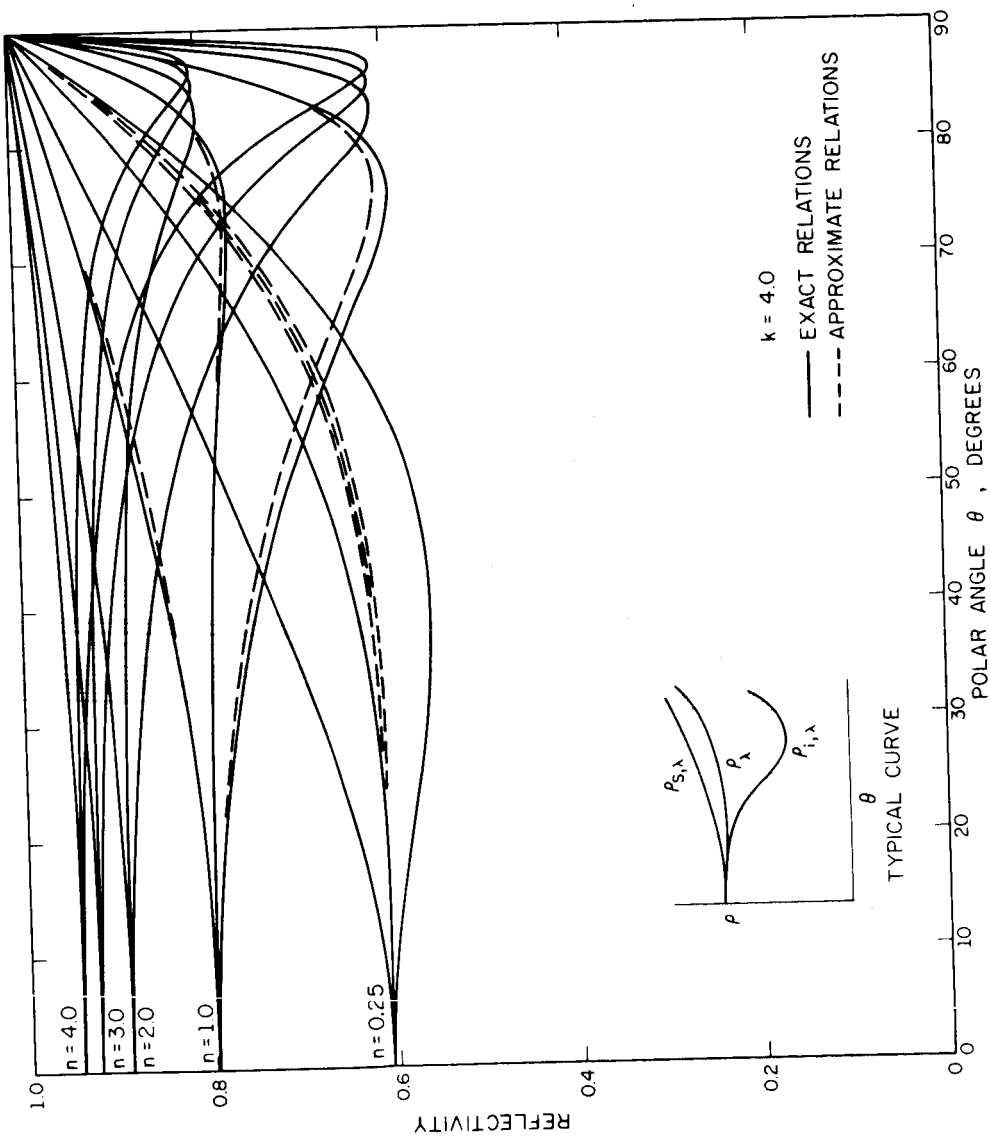

Fig. 9 Directional reflectivity for selected values of n (k = 4.0).

accuracy of a certain calculation warrants only a 5.0 per cent accuracy in the directional reflectivity, the approximate formulae of Eqs. (3.2.6) and (3.2.7) may be used to evaluate the reflectivity for unpolarized radiation provided $n^2(1 + k^2) \geq 7$ if $n \geq 1$. On the other hand, if polarization effects are of importance, $n^2(1 + k^2)$ must exceed 70 when $n \geq 1$ to assure a 5.0 per cent accuracy in the calculation of $\rho_{i,\lambda}(\theta)$. Should the material exhibit values of $n^2(1 + k^2) < 7$, then there is no alternative but to use the exact relations to achieve the desired accuracy.

The normal emissivity has received considerable attention in the literature. This may be generally attributed to the ease with which it may be measured in comparison to, for example, the hemispherical emissivity. The normal emissivity, $\epsilon_{N,\lambda}$ is the directional emissivity evaluated in the direction of the surface normal ($\theta = 0$). The approximate formulae yield the value derived from the exact relations, that is,

$$\epsilon_{N,\lambda} = \epsilon_\lambda(0) = \frac{4}{(n + 1)^2 + n^2k^2}$$

The dependence of $\epsilon_{N,\lambda}$ on the optical parameters n and k is illustrated in Figures 10 and 11.

TABLE 2

MINIMUM ALLOWABLE VALUES OF $n^2(1 + k^2)$ FOR SELECTED ACCURACY IN APPROXIMATE REFLECTIVITY RELATIONS

PERCENT ACCURACY	1.0		5.0		10.0	
REFRACTIVE INDEX	$n < 1$	$n \geq 1$	$n < 1$	$n \geq 1$	$n < 1$	$n >$
$\rho_\lambda(\theta)$	4	25	3	7	2	5
$\rho_{s,\lambda}(\theta)$	15	25	6	7	5	5
$\rho_{i,\lambda}(\theta)$	40	200	11	70	5	40

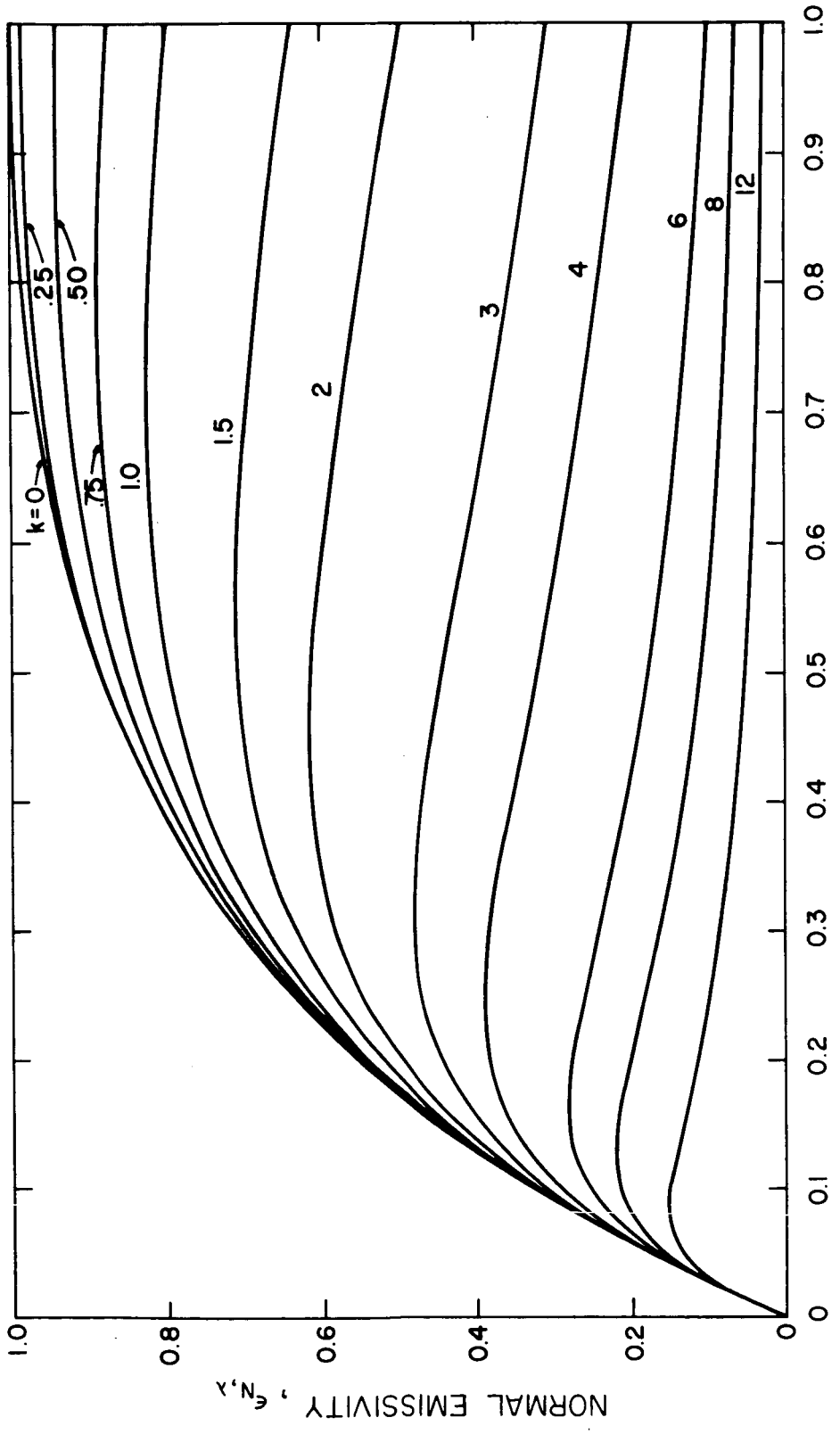

Fig. 10 Normal emissivity ($n \leq 1.0$).

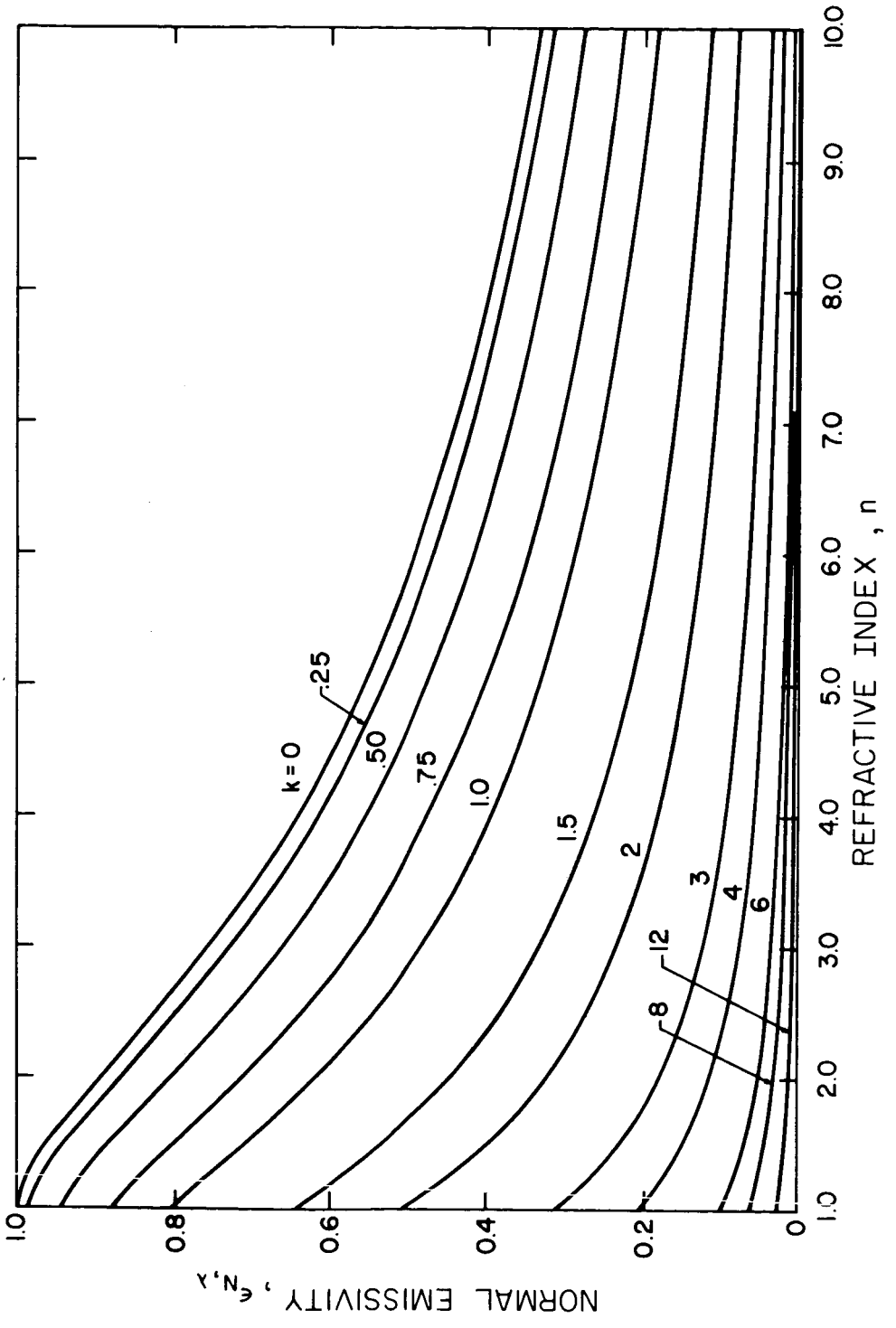

Fig. 11 Normal emissivity ($n \geq 1.0$).

3.3 Hemispherical Properties

The relations of electromagnetic theory for directional reflectivity of optically smooth uncontaminated surfaces may also be used to evaluate the monochromatic hemispherical emissivity, $\epsilon_{H,\lambda}$. The hemispherical emissivity may be determined from the directional emissivity by integration over hemispherical space.

$$\epsilon_{H,\lambda} = \int_0^{\pi/2} \epsilon_\lambda(\theta) \sin 2\theta \, d\theta \tag{3.3.1}$$

Account has been taken in Eq. (3.3.1) for the azimuthal symmetry of $\epsilon_\lambda(\theta)$

Analytical integration of the exact relationships for $\epsilon_\lambda(\theta)$ for arbitrary n and k does not appear possible. However, for electrical non-conductors (k = 0) the following closed form may be obtained:

$$\epsilon_{H,\lambda} = \frac{1}{2} - \frac{(3n+1)(n-1)}{6(n+1)^2} - \frac{n^2(n^2-1)^2}{(n^2+1)^3} \ln\left(\frac{n-1}{n+1}\right) + \frac{2n^3(n^2+2n-1)}{(n^4-1)(n^2+1)} - \frac{8n^4(n^4+1)}{(n^2+1)(n^4-1)^2} \ln n \tag{3.3.2}$$

The approximate formulae for $n^2(1+k^2) >> 1$, namely Eqs. (3.2.6) and (3.2.7), yield the following analytical result for hemispherical emissivity for arbitrary n and k:

$$\epsilon_{H,\lambda} = 4n + \frac{4}{n(1+k^2)} - 4n^2 \ln\left[\frac{1+2n+n^2(1+k^2)}{n^2(1+k^2)}\right] - \frac{4}{n^2(1+k^2)^2} \ln\left[1+2n+n^2(1+k^2)\right] + \frac{4n^2(1-k^2)}{k} \tan^{-1}\left[\frac{k}{1+n(1+k^2)}\right] + \frac{4(1-k^2)}{n^2k(1+k^2)^2} \tan^{-1}\left[\frac{nk}{n+1}\right] \tag{3.3.3}$$

A comparison of the results for hemispherical emissivity obtained by numerical integration of the exact relations and those evaluated from Eq. (3.3.3) is shown in Figures 12 and 13 for refractive index values less than and greater than unity, respectively. A range of values for absorption index is considered in each figure. For values of n greater than unity, the discrepancy in results is indistinguishable on Figure 13 provided k exceeds 0.50. The largest error incurred by the use of Eq. (3.3.3) for $n \geq 1$ is 9.0 per cent at $n = 1$ and $k = 0$. For values of the refractive index less than unity, errors of an order of magnitude are incurred by the use of Eq. (3.3.3) for small values of refractive index. Fortunately, most materials with refractive indices less than unity possess large values for the absorption index so that Eq. (3.3.3) is again adequate except possibly for refractive indices less than about 0.1.

Quantitative criteria have been developed for the use of Eq. (3.3.3) in evaluating hemispherical emissivity when the refractive and absorption index are specified in terms of the parameter $n^2(1 + k^2)$. These are given in Table 3 and are used in the same manner as those previously given in Table 2 for the approximate directional reflectivity relations.

TABLE 3

MINIMUM ALLOWABLE VALUES OF $n^2(1 + k^2)$
FOR SELECTED ACCURACY IN APPROXIMATE
HEMISPHERICAL EMISSIVITY RELATION

PERCENT ACCURACY	2.0		5.0	
REFRACTIVE INDEX	$n < 1$	$n \geq 1$	$n < 1$	$n \geq 1$
$^{e}H,\lambda$	3	4	2	1.5

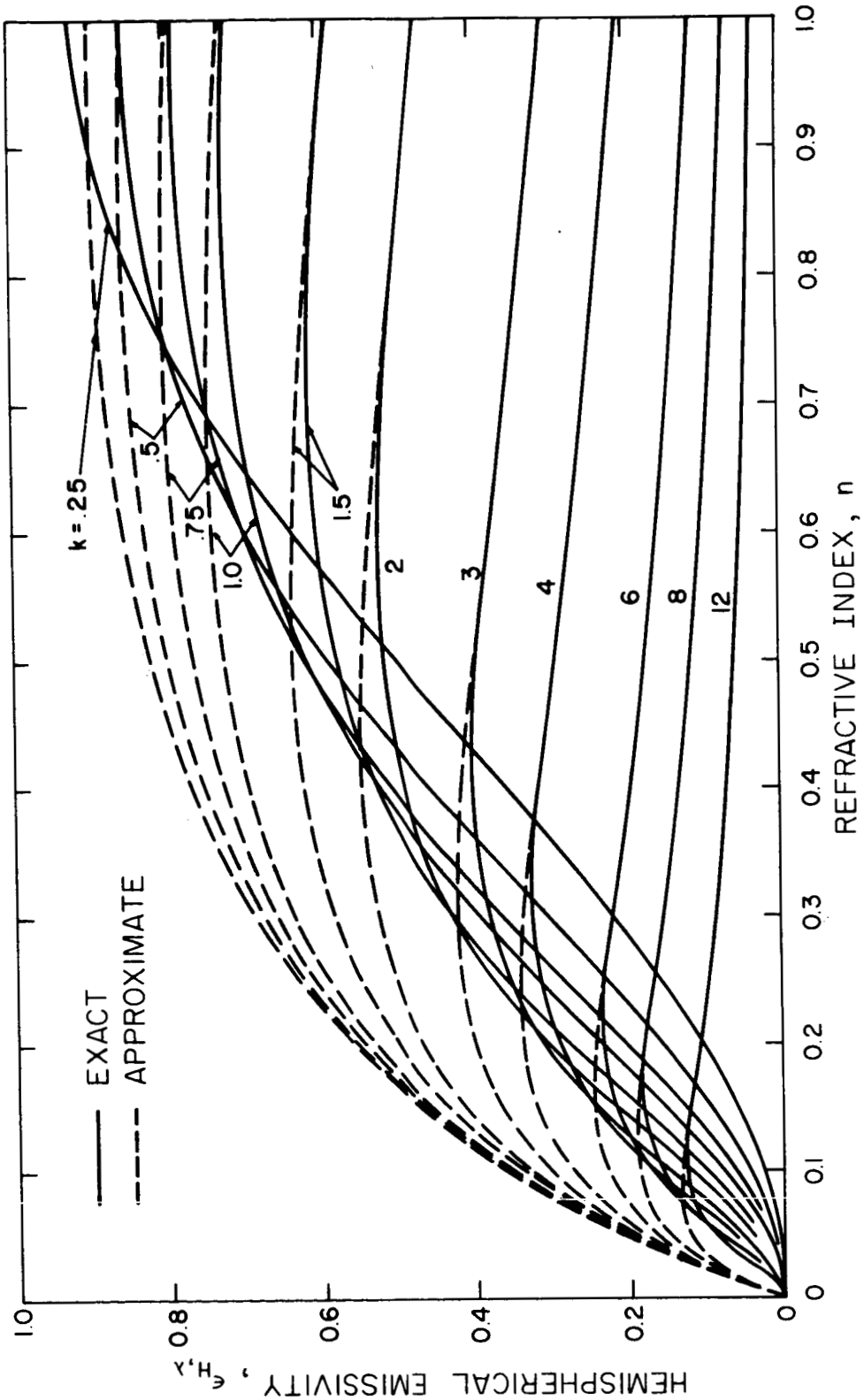

Fig. 12 Comparison of exact and approximate results for hemispherical emissivity ($n \leq 1.0$).

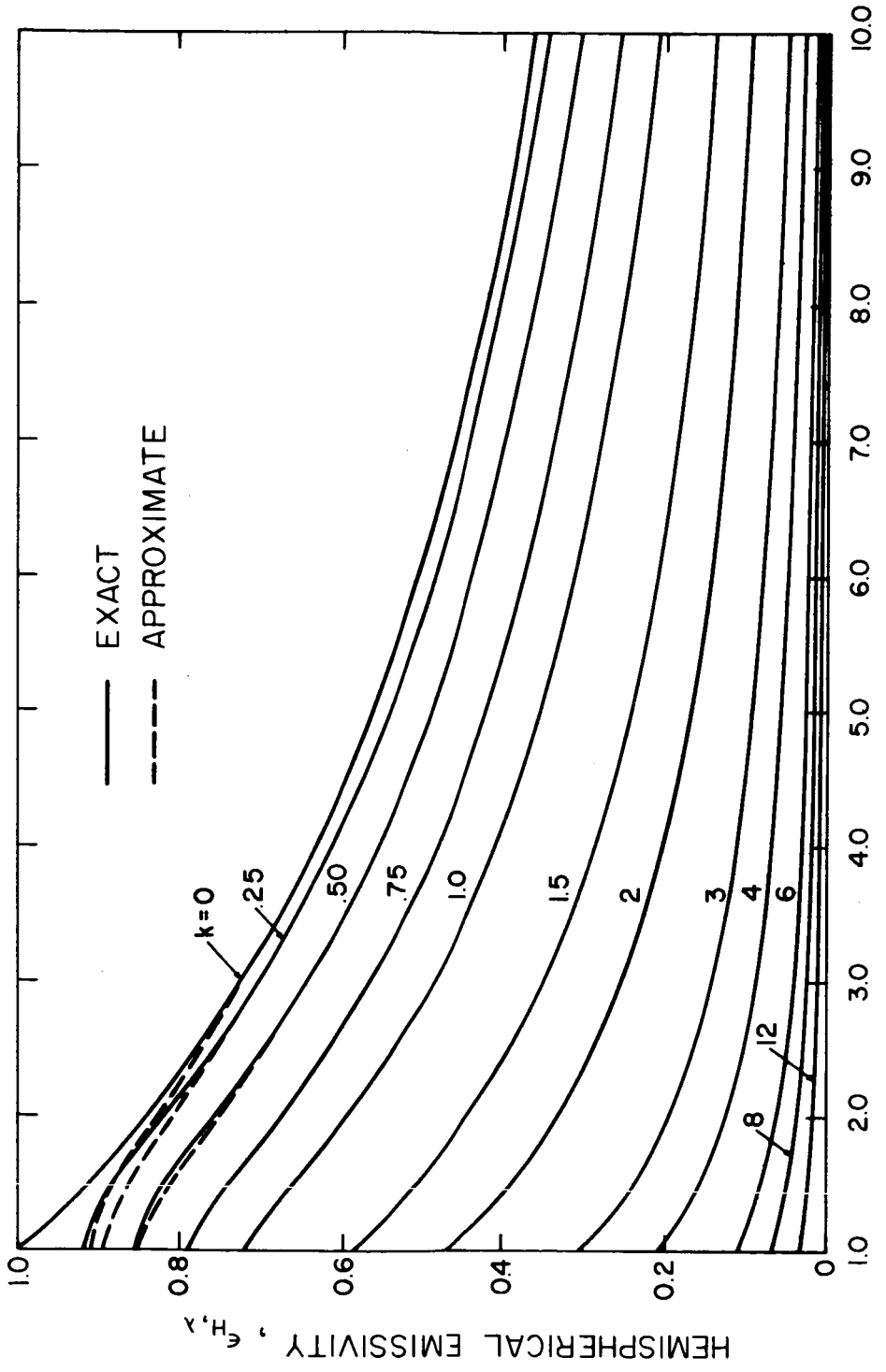

Fig. 13 Comparison of exact and approximate results for hemispherical emissivity ($n \geq 1.0$).

The results for monochromatic normal emissivity of Section 3.2 and those for monochromatic hemispherical emissivity presented here may be utilized to construct curves of $\epsilon_{H,\lambda}/\epsilon_{N,\lambda}$ verses $\epsilon_{N,\lambda}$. Such curves are particularly useful for the determination of the optical constants of materials. Measurements of the spectral normal and spectral hemispherical emissivity of an optically smooth uncontaminated plane sample suffices to determine n and k at the wave length of the measurement. With this in mind, Figures 14, 15, and 16 have been constructed from the results of the exact relations. The complicated character of $\epsilon_{H,\lambda}/\epsilon_{N,\lambda}$ versus $\epsilon_{N,\lambda}$ curves requires a number of figures to adequately display the results. Figures 14 and 15 illustrate the results for absorption index values between 0.0 and 20.0 for refractive indices less and greater than unity, respectively. The experimental values of n and k for electrical conductors are such that $\epsilon_{N,\lambda}$ is often less than 0.2. Since this portion of Figure 15 is difficult to interpret, it is shown at a smaller scale in Figure 16.

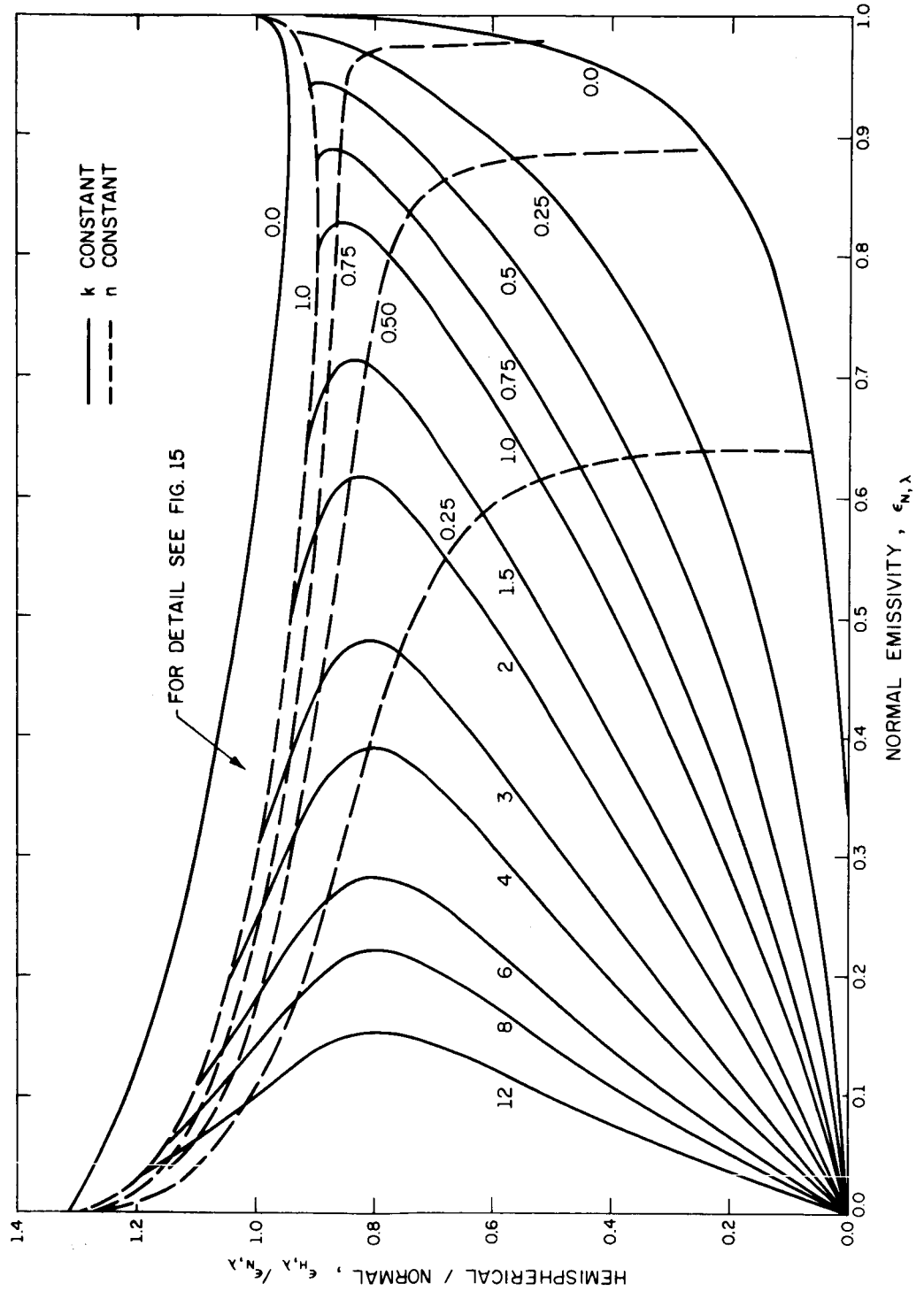

Fig. 14 Ratio of hemispherical to normal emissivity as a function of normal emissivity.

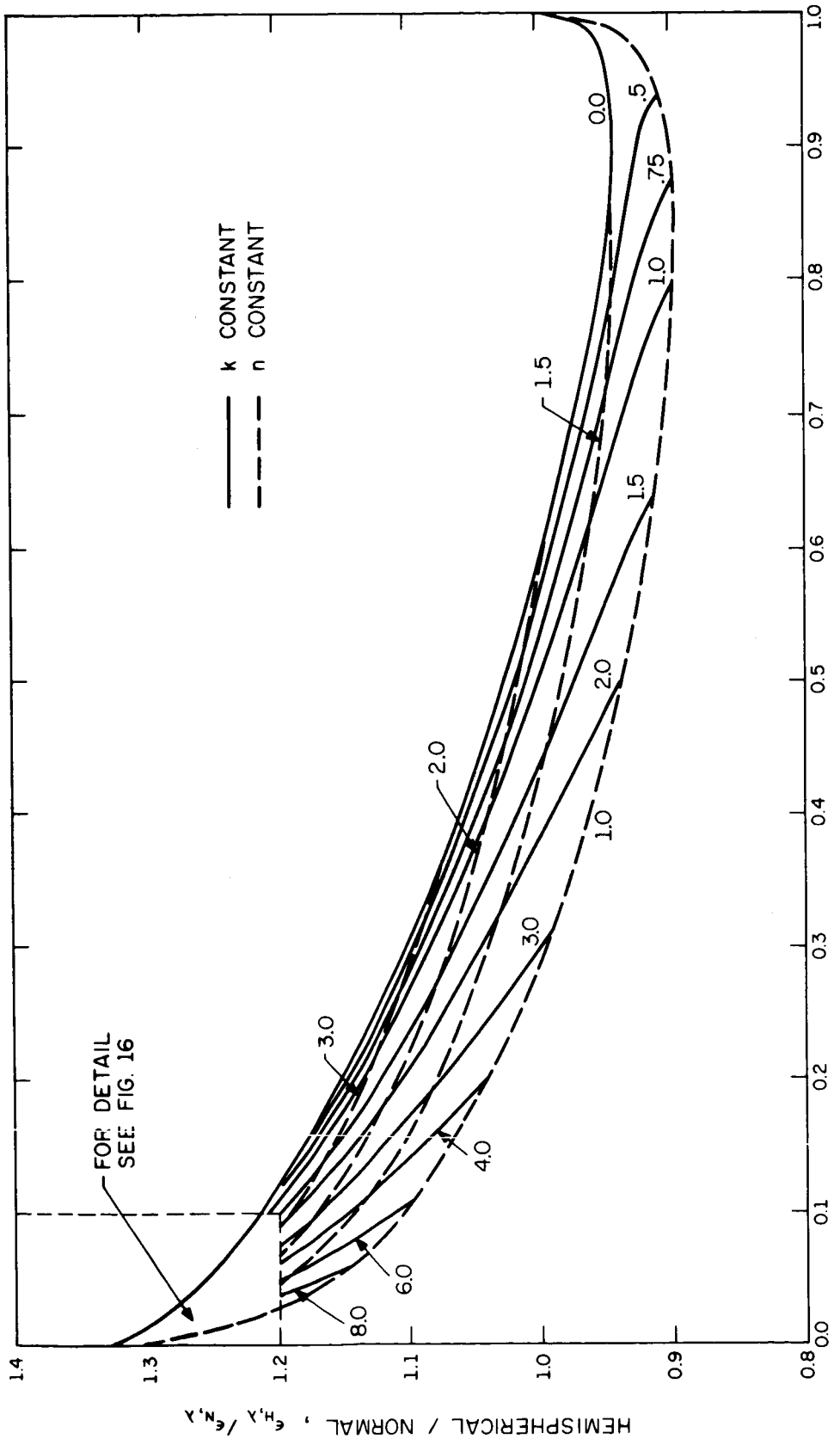

Fig. 15 Ratio of hemispherical to normal emissivity as a function of normal emissivity.

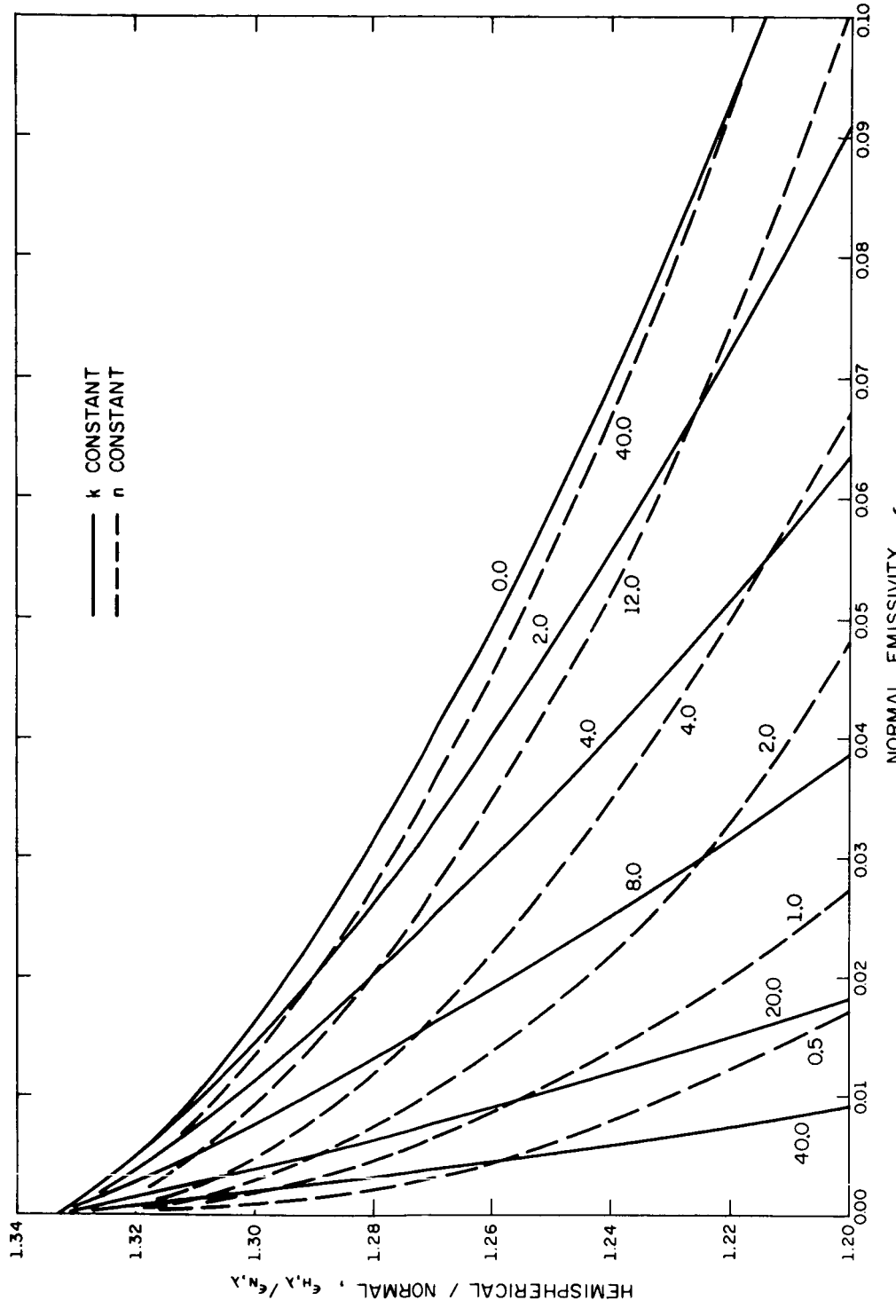

Fig. 16 Ratio of hemispherical to normal emissivity as a function of normal emissivity.

4.0 Heat Transfer and Equilibrium Temperatures

The non-gray non-diffuse surface heat transfer study has not progressed to the point where heat transfer results are available. However, intensity distributions have been calculated using the Beckmann bi-directional reflectance model in the strip system illustrated in Fig. 17. These show significant departures from those of diffuse and specular surfaces. Section 4.1 is devoted to a discussion of these results.

As previously indicated, the accuracy of the commonly employed gray theories for heat transfer will be assessed by comparison of heat transfer and equilibrium temperatures predicted by these with that of the comprehensive real surface analysis in progress. Unfortunately, the gray theory results available are insufficient for a meaningful comparison. As a result of this deficiency, an effort was initiated to supplement the available analyses with those required for this study. The system considered in each case is that of Fig. 2.

In way of review, the assumptions employed in the gray analysis include the neglect of end effects (infinite width plates) for equal length opaque plates exchanging radiant energy in the absence of an attenuating media but in the presence of a collimated solar field. The properties of each surface are taken uniform over the extent of each surface. The prescribed temperature distribution for radiant flux calculation as well as the prescribed flux distribution for temperature determination will be restricted to a spatial variation only in the distance measured normal to the common apex. Under the prescribed conditions, the local heat flux for surfaces of prescribed temperature and the local temperature for surfaces of specified local radiant flux also depends only on the coordinate along the plate length. The analysis for diffusely emitting-diffusely reflecting surfaces is summarized in Section

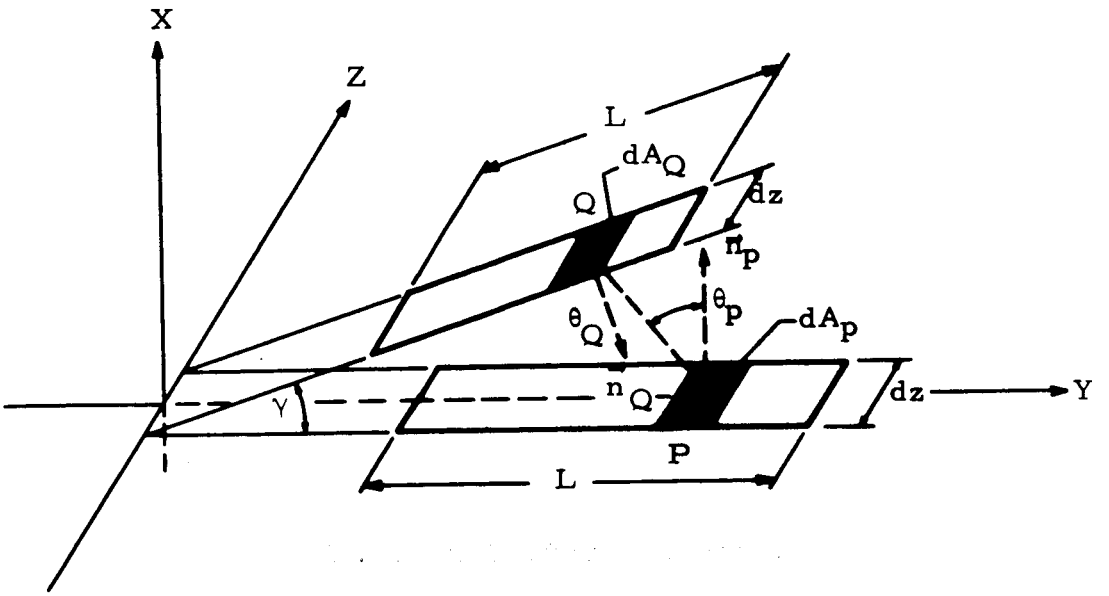

Fig. 17 Thin strips geometry.

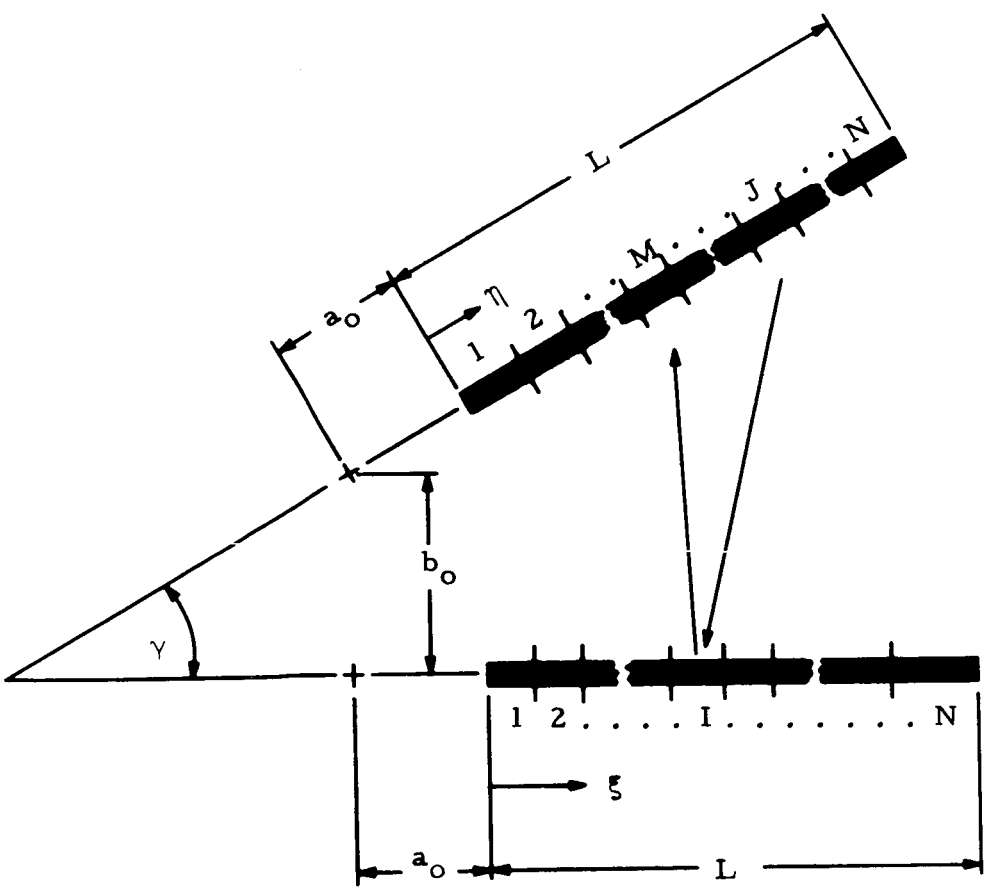

Fig. 18 Finite difference form of thin strips geometry.

4.2.1 while that for diffusely emitting-specularly reflecting surfaces is presented in Section 4.2.2. Equilibrium temperature distributions for the adjoint plate system ($a_o = b_o = 0$) in a solar field directed along the bisector of the included angle ($\theta_s = \frac{\pi - \gamma}{2}$) for both analyses are presented and discussed in Section 4.2.3.

The analysis of Section 4.2 neglects the dependence of radiative surface properties on direction of incident or emitted radiation. The heat transfer results of a gray analysis for specularly reflecting surfaces of uniform temperature which includes the directional dependence of emissivity, absorptivity, and reflectivity are reviewed in Section 4.3. The details of this analysis are available in the literature [3].

4.1 Non-gray Non-diffuse Surfaces

This section is devoted to the presentation and discussion of representative samples of initial results obtained from the non-gray, non-diffuse radiant heat exchange analysis. Although the investigation is not complete, results are available which indicate that significant deviations from gray diffuse or gray specular results can be expected. The importance of a complete characterization of surface roughness is also demonstrated.

The results presented here are spectral intensity distributions calculated for the thin, adjoint strips geometry (Figure 17) with given uniform and equal surface temperatures and no external flux. The directional emittance is that predicted by the Fresnel relations, and for present purposes it is assumed that variations of the refractive and absorption indices with wave length are small enough to be neglected. For wave lengths in the infrared this should be reasonably valid.

Numerical solutions were obtained with each strip divided into ten equal length elements (Figure 18). The width of the strips was taken as one tenth the strip length. The numerical solution yields, for each element the intensities in the directions along lines drawn from the center of the given element to the center of each of the ten elements on the opposite strip. It must be emphasized that the results presented here are preliminary and only qualitative remarks can be made concerning them. Much work remains before quantitative results can be given. An important factor to be evaluated is the truncation error introduced by the finite subdivision of the system.

If an accurate semigray model for radiant exchange is to be developed,

it is necessary to determine the affect of surface roughness on radiant exchange for the range of the spectrum of interest. The results shown on Figure 19 are for this purpose. The strip surfaces were assumed to have fixed roughness parameters σ and a as required by the Beckmann reflectance model. Intensity distributions were then calculated for emission at several different wave lengths. The particular parameter values selected are indicated on the figure. For these calculations the directional emissivity was taken to be that predicted by the Fresnel relations for $n = 9.25$ and $k = 2.0$. These values yield a spectral hemispherical emissivity of 0.1. Intensities were also calculated for smooth (specular) surfaces with directional emissivity as described above, and for diffusely reflecting and emitting surfaces with spectral hemispherical emissivity of 0.1.

The results shown on Figure 19 for element four indicate that significant variations in intensity distribution (local radiant flux) can occur for various portions of the spectrum. That is, even though n and k have been assumed independent of wave length, the radiant exchange appears non-gray due to roughness affects. It is observed that as the wave length increases (σ/λ and a/λ decrease) the intensity distributions approach that for purely specular reflection. These preliminary calculations also indicate that the specular and diffuse results may not represent upper and lower bounds on the local intensity.

It should be recognized that the large dip in the specular curve near the element normal is due to the small number of subdivisions used.

Recently attention has been directed toward determining the surface characteristics necessary for an adequate description of radiation properties. Much of the published data for radiation properties of rough metallic surfaces

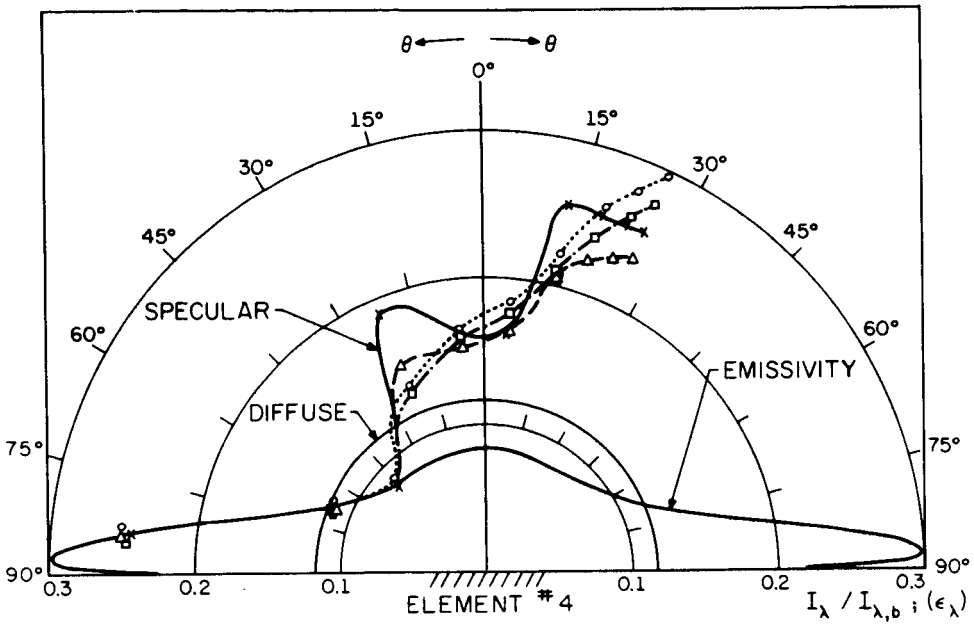

$\frac{a}{\sigma} = 25.0$, $n = 9.25$, $k = 2.00$, $\epsilon_{H,\lambda} = 0.10$, $\gamma = 45°$

$\frac{a_o}{L} = 0.0$, $\frac{b_o}{L} = 0.0$, $\frac{\Delta z}{L} = 0.10$

$\frac{\sigma}{\lambda} = 0.00$ (SPECULAR) $\frac{\sigma}{\lambda} = 0.08$

$\frac{\sigma}{\lambda} = 0.20$ $\frac{\sigma}{\lambda} = 0.50$

Fig. 19 Normalized intensities of element No. 4 with fixed σ and a for several wave lengths.

has been accompanied by only an estimate of optical roughness σ/λ. Figure 20 shows normalized intensity distributions calculated for the strip system with optical roughness fixed at $\sigma/\lambda = 0.2$ and for two values of correlation distance $a/\lambda = 5.0$ and 15.0. The strong influence of the correlation distance a on the intensity distribution indicates that specification of optical roughness by itself is insufficient to allow accurate local radiant exchange predictions.

4.2 Gray Surfaces--Directionally Independent Properties

Both the analyses of Section 4.2 consider gray diffusely emitting surfaces with the limiting cases of diffuse (Sec. 4.2.1) and specular (Sec. 4.2.2) reflection. No account is taken for the directional dependence of surface properties in either analysis.

4.2.1 Diffusely Emitting--Diffusely Reflecting Surfaces

An analysis is briefly described which effectively reduces the evaluation of local radiant heat loss or temperature to the determination of the solution to two simultaneous linear integral equations. It is demonstrated that under certain conditions the governing integral equations may be simplified to two pairs of integral equations whose solution depends only on the surface properties and included angle. Equilibrium surface temperature distributions for the adjoint plate system derived from the analysis are presented in Section 4.2.3.

Consider first the evaluation of local radiant heat loss for the surfaces when the temperature distribution on each is specified. The steady radiant transfer rate from an element dA_i of plate i (i = 1 or 2) is the difference between the rates at which energy is emitted and incident energy

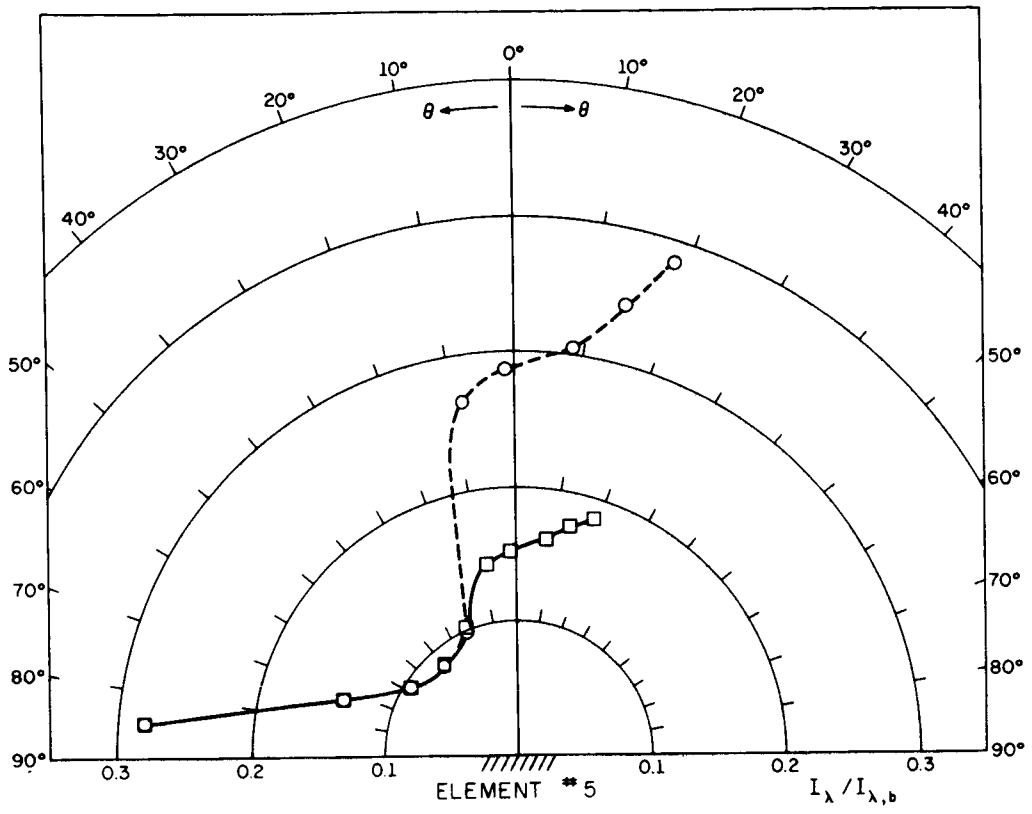

$\frac{\sigma}{\lambda} = 0.20$

$\frac{a}{\lambda} = 5.0$ $\frac{a}{\lambda} = 15.0$

$n = 9.25$, $k = 2.00$, $\epsilon_{H,\lambda} = 0.10$, $\gamma = 45°$

$\frac{a_o}{L} = 0.0$, $\frac{b_o}{L} = 0.0$, $\frac{\Delta z}{L} = 0.10$

Fig. 20 Normalized intensities of element No. 5 with fixed σ/λ for two values of a/λ.

absorbed. On a unit area basis, the net radiant heat loss per unit time of the considered element, q_i'', may be expressed as

$$q_i''(x_i) = \frac{\epsilon_i}{1-\epsilon_i}\left[E_{b,i}(x_i) - B_i(x_i)\right], \qquad (4.2.1)$$

$$(i = 1, 2)$$

where $E_{b,i}$, B_i, ϵ_i represent local black body emissive power, radiosity, and emissivity, respectively.

If the local radiant heat loss is specified, Eq. (4.2.1) may be rearranged to yield the local temperature.

$$\sigma T_i^4(x_i) = \left(\frac{1-\epsilon_i}{\epsilon_i}\right) q_i''(x_i) + B_i(x_i), \qquad (4.2.2)$$

$$(i = 1, 2)$$

In Eq. (4.2.2), σ is the Stefan-Boltzmann constant.

In either surface condition, that is, specified temperature or specified heat flux, the evaluation of the quantity of interest (heat flux or temperature) is readily calculated once the radiosity distribution has been evaluated. With this in mind, attention is turned to the determination of the radiosity.

The radiosity of an element of surface i, $B_i(x_i)$, is the sum of the rate of emission and rate at which incident radiant energy is reflected. The incident energy consists of the sum of contributions due to diffuse energy leaving plate j ($j \neq i$) and direct illumination by the collimated solar field. Thus

$$B_i(x_i) = \epsilon_i E_{b,i}(x_i) + (1 - \epsilon_i)\left[\int_j B_j(x_j) K_\gamma(x_i, x_j)\, dx_j + SF_i(x_i)\right], \qquad (4.2.3)$$

$$\begin{pmatrix} i = 1, 2 \\ j = 1, 2 \end{pmatrix} \quad i \neq j$$

where

$$K_\gamma(x_i,x_j) = \frac{\sin^2\gamma}{2} \quad \frac{x_i x_j}{[x_i^2 + x_j^2 - 2x_i x_j \cdot \cos\gamma]^{3/2}} \tag{4.2.4}$$

The integral appearing in Eq. (4.2.3) represents the contribution of the adjacent plate to the incident energy and $SF_i(x_i)$ the direct illumination due to the solar field. S remains the value of the solar flux measured normal to the collimated field on a unit area surface. $F_i(x_i)$ accounts for the spatial variation of the directly incident solar flux on the surfaces. As an example, $F_i(x_i)$ is given by the relation

$$F_i(x_i) = \sin\frac{\gamma}{2}, \qquad (i = 1, 2) \tag{4.2.5}$$

for fully illuminated surfaces.

For surfaces with specified radiant flux, Eq. (4.2.2) may be used to eliminate $E_{b,i}(= \sigma T_i^4)$ in favor of the known flux $q_i''(x_i)$ to yield

$$B_i(x_i) = q_i''(x_i) + \left[\int_j B_j(x_j)\, K_\gamma(x_i,x_j)\, dx_j + S\, F_i(x_i)\right], \tag{4.2.6}$$

$$\begin{pmatrix} i = 1, 2 \\ j = 1, 2 \end{pmatrix} \quad i \neq j$$

Both pairs of integral equations, that is, those for specified temperature distribution (Eq. (4.2.3)), and those for specified surface heat flux (Eq. (4.2.6)), are included in the general form

$$B_i(x_i) = G_i(x_i) + C_i \int_j B_j(x_j)\, K_\gamma(x_i,x_j)dx_j, \tag{4.2.7}$$

$$\begin{pmatrix} i = 1, 2 \\ j = 1, 2 \end{pmatrix} \quad i \neq j$$

For surfaces with specified temperature distribution

$$C_i = 1 - \epsilon_i, \quad G_i(x_i) = \epsilon_i E_{b,i}(x_i) + C_i S F_i(x_i) \tag{4.2.8}$$

while for surfaces of specified local radiant heat loss

$$C_i = 1, \quad G_i(x_i) = q_i''(x_i) + S F_i(x_i) \tag{4.2.9}$$

The solution of the simultaneous linear integral equations, Eq. (4.2.7), depends on a number of parameters including the properties of the plates, included angle, solar field magnitude and direction, and either the distribution of temperature or radiant heat transfer along the surfaces.

Considerable simplification may be realized in the system, Eq. (4.2.7), when the functions G_i are non-zero constants. In particular, it may be shown that the radiosities B_i are given by

$$B_i(x_i) = G_i \beta_{ia}(\xi_i) + G_j \beta_{ib}(\xi_i), \qquad \begin{pmatrix} i = 1, 2 \\ j = 1, 2 \end{pmatrix} \quad i \neq j \tag{4.2.10}$$

where the dimensionless radiosities β_{ia} and β_{jb} are determined by the simultaneous integral equations

$$\begin{aligned} \beta_{ia}(\xi_i) &= 1 + C_i \int_{\xi_j} \beta_{jb}(\xi_j) K_\gamma (\xi_i, \xi_j) \, d\xi_j \\ \beta_{jb}(\xi_j) &= C_j \int_{\xi_i} \beta_{ia}(\xi_i) K_\gamma (\xi_i, \xi_j) \, d\xi_i \end{aligned} \qquad \begin{pmatrix} i = 1, 2 \\ j = 1, 2 \end{pmatrix} \quad i \neq j \tag{4.2.11}$$

The solution of Eqs. (4.2.11) depends only on the included angle and properties of the plates. For surfaces with specified radiant heat flux, the parameter dependence reduces to only the included angle.

The simplifications which result when the G_i are non-zero constants

pertain to some important situations. The directly incident solar radiation is uniform for a fully illuminated system and a semi-illuminated system in which one surface is completely illuminated and the other receives no direct solar illumination. Of course, the trivial case of no direct illumination is also a possibility. For these conditions of exposure to the solar field, the G_i are constant provided the surface temperatures or radiant heat transfer is uniform. Equilibrium temperatures may be determined in the latter case only for fully illuminated surfaces.

In summary, when both surfaces have uniform but not necessarily identical temperatures and are exposed to the collimated solar field such that the system is fully- or semi-illuminated, the dimensionless local radiant heat loss of either surface may be evaluated from the relation

$$\frac{q_i''(x_i)}{\epsilon_i \sigma T_{ref}^4} = \frac{1}{(1 - \epsilon_1)} \left[\left(\frac{T_i}{T_{ref}}\right)^4 - \left\langle \epsilon_i \left(\frac{T_i}{T_{ref}}\right)^4 + (1 - \epsilon_i) \left(\frac{S}{\sigma T_{ref}^4}\right) F_i \right\rangle \beta_{ia} - \left\langle \epsilon_j \left(\frac{T_j}{T_{ref}}\right)^4 + (1 - \epsilon_j) \left(\frac{S}{\sigma T_{ref}^4}\right) F_i \right\rangle \beta_{ib} \right]$$

$$\begin{pmatrix} i = 1, 2 \\ j = 1, 2 \end{pmatrix} \quad i \neq j \qquad (4.2.12)$$

where T_{ref} is an arbitrary reference temperature. For surfaces of constant local radiant heat loss under the same conditions of solar illumination, the local temperature may be evaluated from the result

$$\left(\frac{T_i(x_i)}{T_{ref}}\right)^4 = \left(\frac{1 - \epsilon_i}{\epsilon_i}\right)\left(\frac{q_i''}{\sigma T_{ref}^4}\right) + \left\langle \left(\frac{q_i''}{\sigma T_{ref}^4}\right) + \left(\frac{S}{\sigma T_{ref}^4}\right) F_i \right\rangle \beta_{ia} + \left\langle \left(\frac{q_j''}{\sigma T_{ref}^4}\right) + \left(\frac{S}{\sigma T_{ref}^4}\right) F_j \right\rangle \beta_{ib}$$

$$\begin{pmatrix} i = 1, 2 \\ j = 1, 2 \end{pmatrix} \quad i \neq j \qquad (4.2.13)$$

The dimensionless radiosities β_{ia} and β_{ib} $(i = 1,2)$ are the solutions to Eq. (4.2.11).

4.2.2 Diffusely Emitting-Specularly Reflecting Surfaces

An analysis is presented for the evaluation of local radiant heat flux or temperature of gray diffusely emitting-specularly reflecting surfaces. It is shown that the local radiant flux for surfaces of specified temperature distribution may be directly calculated. Equilibrium temperature distribution for surfaces of zero radiant heat flux requires the solution of simultaneous linear integral equations. Equilibrium temperature results obtained from the analysis are given in Section 4.2.3.

Again, consideration is initially given to the evaluation of local radiant heat loss for surfaces of specified temperature distribution. The steady radiant transfer rate from element dA_i of plate i (i = 1 or 2) is the difference between the rates at which energy is emitted and incident energy absorbed. On a unit area basis, the net radiant heat loss per unit time of the considered element, $q_i''(x_i)$, may be expressed as

$$q_i''(x_i) = \epsilon_i \left[E_b(x_i) - H_i(x_i)\right], \quad (i = 1,2) \quad (4.2.14)$$

where H_i represents the local irradiation.

If local radiant heat loss is specified, Eq. (4.2.14) may be rearranged to yield the local temperature.

$$\sigma T_i^4(x_i) = \frac{q_i''(x_i)}{\epsilon_i} + H_i(x_i) \qquad (i = 1,2) \quad (4.2.15)$$

Thus the evaluation of local radiant heat loss for surfaces with specified temperature distribution or surface temperature distribution for surfaces of

specified local heat flux requires the determination of the local irradiation $H_i(x_i)$. Attention is therefore directed to the evaluation of $H_i(x_i)$.

The irradiation of an element of surface i, $H_i(x_i)$, consists of contributions due to both surfaces and the collimated solar field. The contribution of each source may be evaluated by accounting for the energy directly transported and that arriving by all possible specular reflections. The latter may be determined by employing the imaging techniques currently in widespread use. The result of such analysis is an expression of the following form:

$$H_i(x_i) = S\,F_i(x_i) + \sum_{j=1}^{2} \int_j \epsilon_j\, E_{b,j}(x_j)\, K_\gamma(x_i,x_j)dx_j, \qquad (4.2.16)$$

$$(i = 1,2)$$

The summation in Eq. (4.2.16) accounts for the emitted energy of both surfaces which arrives by direct transport and specular reflections. The remaining term is the contribution of the collimated solar field which again accounts for direct and specular reflection paths. In general, the function F_i and K_γ depend not only on geometry as in the analysis for diffusely reflecting surfaces of Section 4.2.1, but also on the values for the specular reflectance of both surfaces.

Introducing Eq. (4.2.16) into Eq. (4.2.14) yields the following expression for the local radiant heat flux for surfaces of specified temperature:

$$q_i''(x_i) = \epsilon_i \left[\sigma T_i^4(x_i) - S\,F_i(x_i) - \sum_{j=1}^{2} \sigma \int_j \epsilon_j\, T_j^4(x_j)\, K_\gamma(x_i,x_j)dx_j \right],$$

$$(i = 1,2) \qquad (4.2.17)$$

According to the above result, the local radiant heat flux may be evaluated once the properties of the surfaces, magnitude and direction of the solar field, and the orientation of the surfaces are specified. This is in contrast to the necessity for first determining the solution to auxiliary integral equations in the diffusely reflecting analysis of Section 4.2.1. For surfaces of specified radiant flux, Eq. (4.2.16) may be used to eliminate $H_i(x_i)$ from Eq. (4.2.17).

$$T_i^4(x_i) = \frac{1}{\sigma}\left[\frac{q_i(x_i)}{\epsilon_i} + S\,F_i(x_i)\right] + \sum_{j=1}^{2}\int_j \epsilon_j T_j^4(x_j)\,K_\gamma(x_i,x_j)dx_j,$$

$$(i = 1,2) \qquad (4.2.18)$$

Equations (4.2.18) constitute a pair of simultaneous linear integral equations for the temperature distributions on both surfaces. Their solution depends on the values selected for the properties of both plates $\epsilon_i(\rho_i = 1 - \epsilon_i)$, the variation of local heat flux along each surface, magnitude and direction of collimated solar field, and the geometrical relationships between the surfaces. Further gross simplifications such as those for the diffusely reflecting surface analysis of Section 4.2.1, do not appear possible even for uniform flux except for restricted values of the included angle between the surfaces.

If consideration is limited to the adjoint plate system ($a_o = b_o = 0$) with identical property plates and collimated solar field directed along the bisector of the included angle, the local heat loss for specified temperature and local temperature for specified radiant flux on both surfaces is identical. For this situation, the functions K_γ and F_i are of the following form:

$$K_\gamma(x_i,x_j) \equiv (K_1 + K_2) = f_\gamma + \rho f_{2\gamma} + \rho^2 f_{3\gamma} + \cdots + \rho^k f_{(k+1)\gamma} \tag{4.2.19}$$

$$F_i(x_i) = \sin\frac{\gamma}{2} + \rho\, u_1(x_i' - x_i)\sin\frac{3\gamma}{2} + \rho^2 u_2(x_2' - x_i)\sin\frac{5\gamma}{2} + \cdots + \rho^{m-1} u_{m-1}(x_{m-1}' - x_i)\sin\frac{(2m-1)\gamma}{2} + \rho^m \sin\frac{(2m+1)\gamma}{2} \tag{4.2.20}$$

where

$$f_{n\gamma}(x_i,x_j) = \frac{\sin^2 n\gamma}{2} \frac{x_i x_j}{[x_i^2 + x_j^2 - 2x_i x_j \cos n\gamma]^{3/2}} \tag{4.2.21}$$

$$u_m(z) = \begin{cases} 1, & z \geq 0 \\ 0, & z < 0 \end{cases} \tag{4.2.22}$$

$$\frac{x_m'}{L} = \frac{\sin \gamma/2}{\sin(2m+1)/2} \tag{4.2.23}$$

and ρ denotes the common specular reflectance value of the surfaces. The number of terms in K_γ and F_i, that is the values of k amd m depend on the value of the included angle. Thus, when the surfaces of the system have uniform properties and specified distribution of temperature, the dimensionless local radiant heat flux of either surface may be evaluated from the following relation:

$$\frac{q_i''(x_i)}{\epsilon_i \sigma T_{ref}^4} = \frac{T_i^4(x_i)}{T_{ref}^4} - \left(\frac{S}{\sigma T_{ref}^4}\right) F_i - \sum_{j=1}^{2} \frac{\epsilon_j}{\epsilon_i} \int_j \frac{T_j^4(x_j)}{T_{ref}^4} K_\gamma(x_i,x_j)\,dx_j, \quad (i = 1,2) \tag{4.2.24}$$

For surfaces of constant local radiant heat flux, the local dimensionless temperature is determined by the simultaneous solution of the pair of integral equations

$$\frac{T_i^4(x_i)}{T_{ref}^4} = \left[\frac{1}{\epsilon_i}\left(\frac{q_i''(x_i)}{\sigma T_{ref}^4}\right) + \left(\frac{S}{\sigma T_{ref}^4}\right) F_i(x_i)\right]$$

$$+ \sum_{j=1}^{2} \epsilon_j \int_j \frac{T_j^4(x_j)}{T_{ref}^4} K_\gamma(x_i,x_j)dx_j, \qquad (i = 1,2) \qquad (4.2.25)$$

Equilibrium surface temperatures are determined from Eq. (4.2.25) by equating the local radiant flux to zero.

4.2.3 Equilibrium Temperature

Equilibrium surface temperature distributions have been determined for the adjoint plate system ($a_o = b_o = 0$) with identical property plates exposed to a collimated solar field directed parallel to the bisector of the included angle ($\theta_s = (\pi-\gamma)/2$). In this situation, the temperature distribution is identical on both surfaces. Representative results for both the diffusely emitting-diffusely reflecting and the diffusely emitting-specularly reflecting analyses are shown in Figures 21, 22, and 23 for included angles of 30^o, 90^o, and 120^o, respectively. In each figure are shown distributions for emissivity values of 0.1, 0.5, and 0.9 for specularly reflecting surfaces and the single distribution required for a diffuse surface. The value of the solar constant utilized to construct the figures is $S = 442$ BTU/hr ft^2.

The temperature distributions exhibit some common characteristics which should be expected in view of the variation of local irradiation along the surfaces. First, the maximum temperature occurs at the apex and decreases with

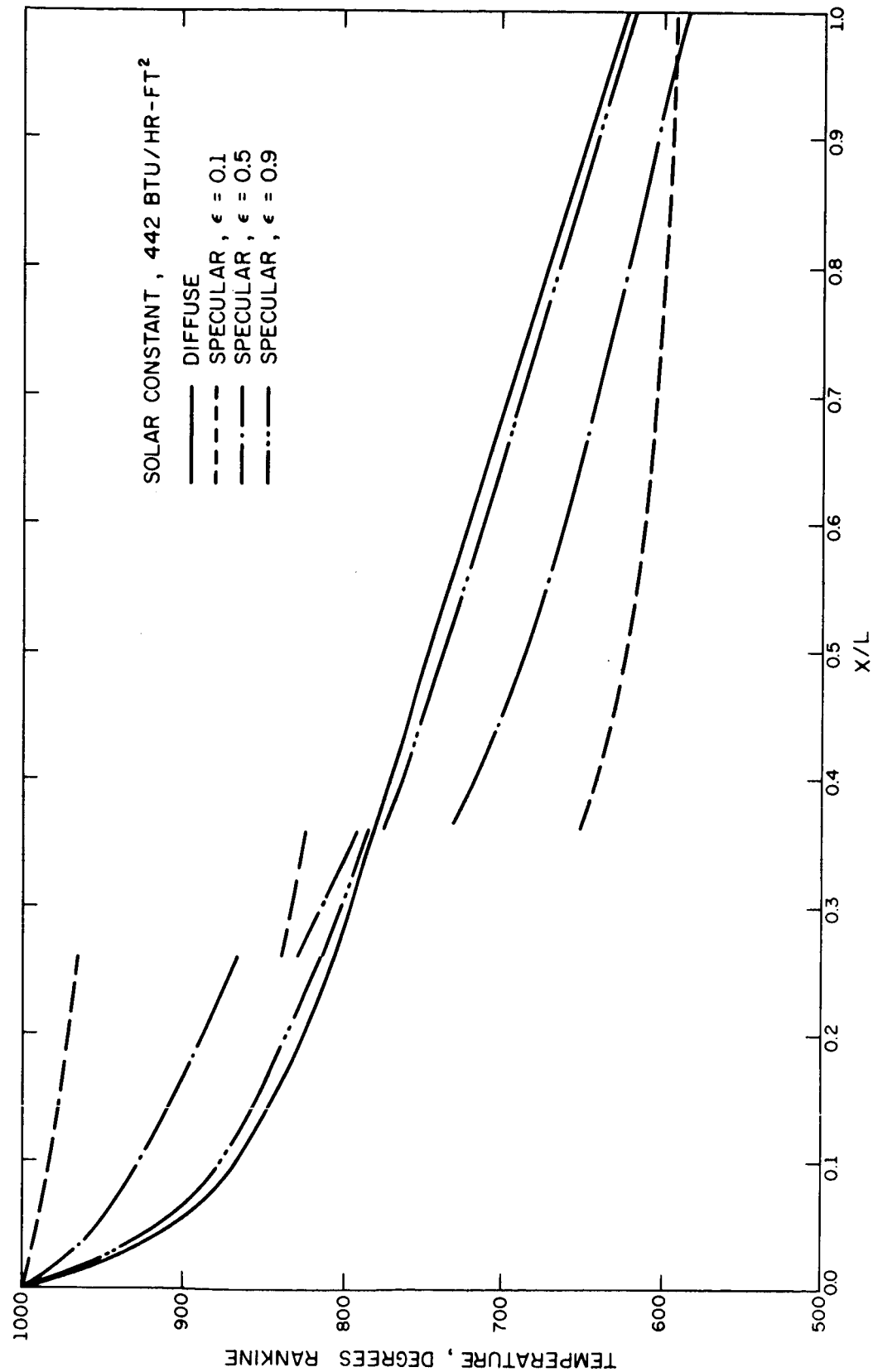

Fig. 21 Equilibrium temperature distributions for the adjoint plate system--gray theory ($\gamma = 30^{\circ}$, $\theta_s = 75^{\circ}$)

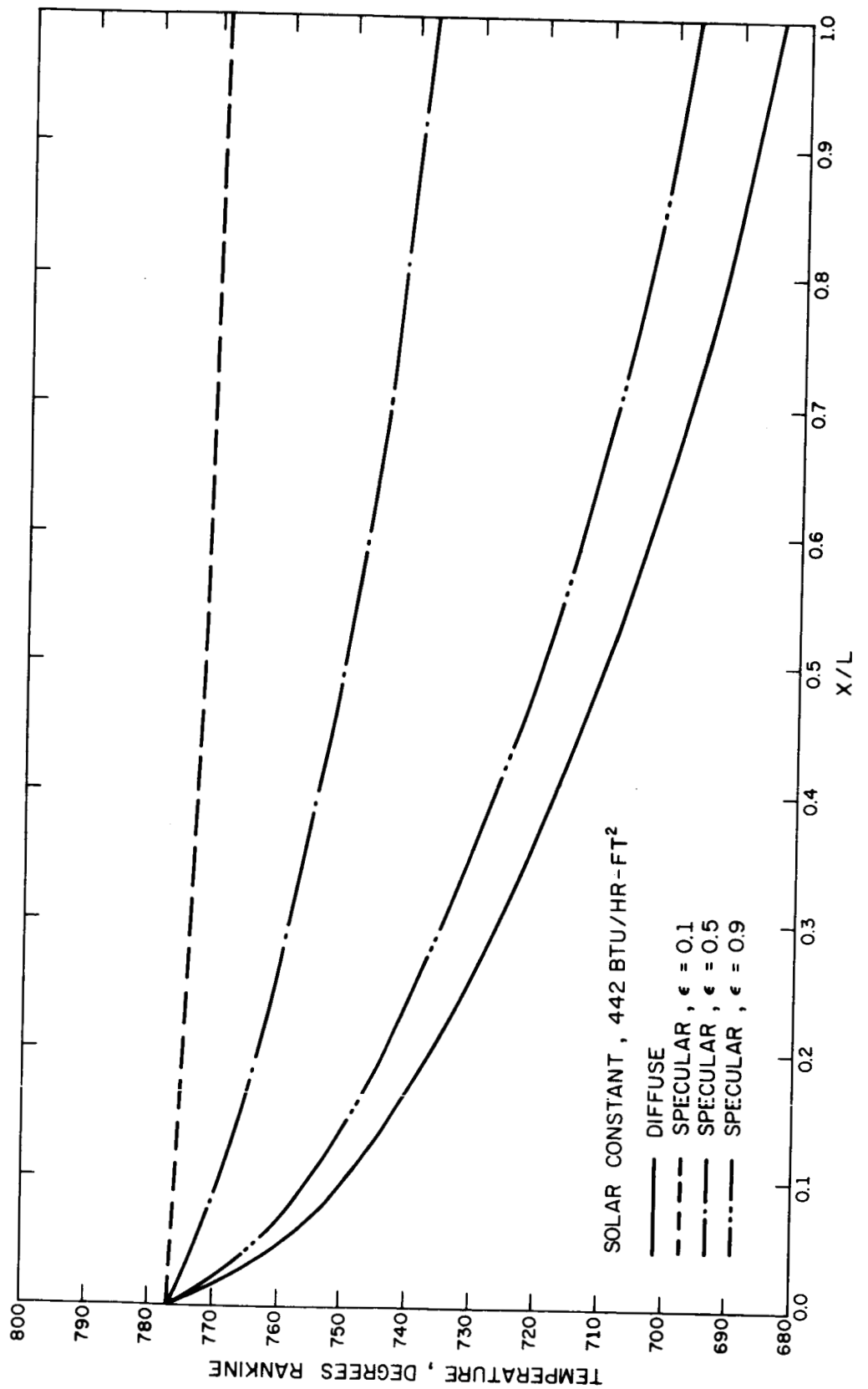

Fig. 22 Equilibrium temperature distributions for the adjoint plate system--gray theory ($\gamma = 90^{o}$, $\theta_s = 45^{o}$)

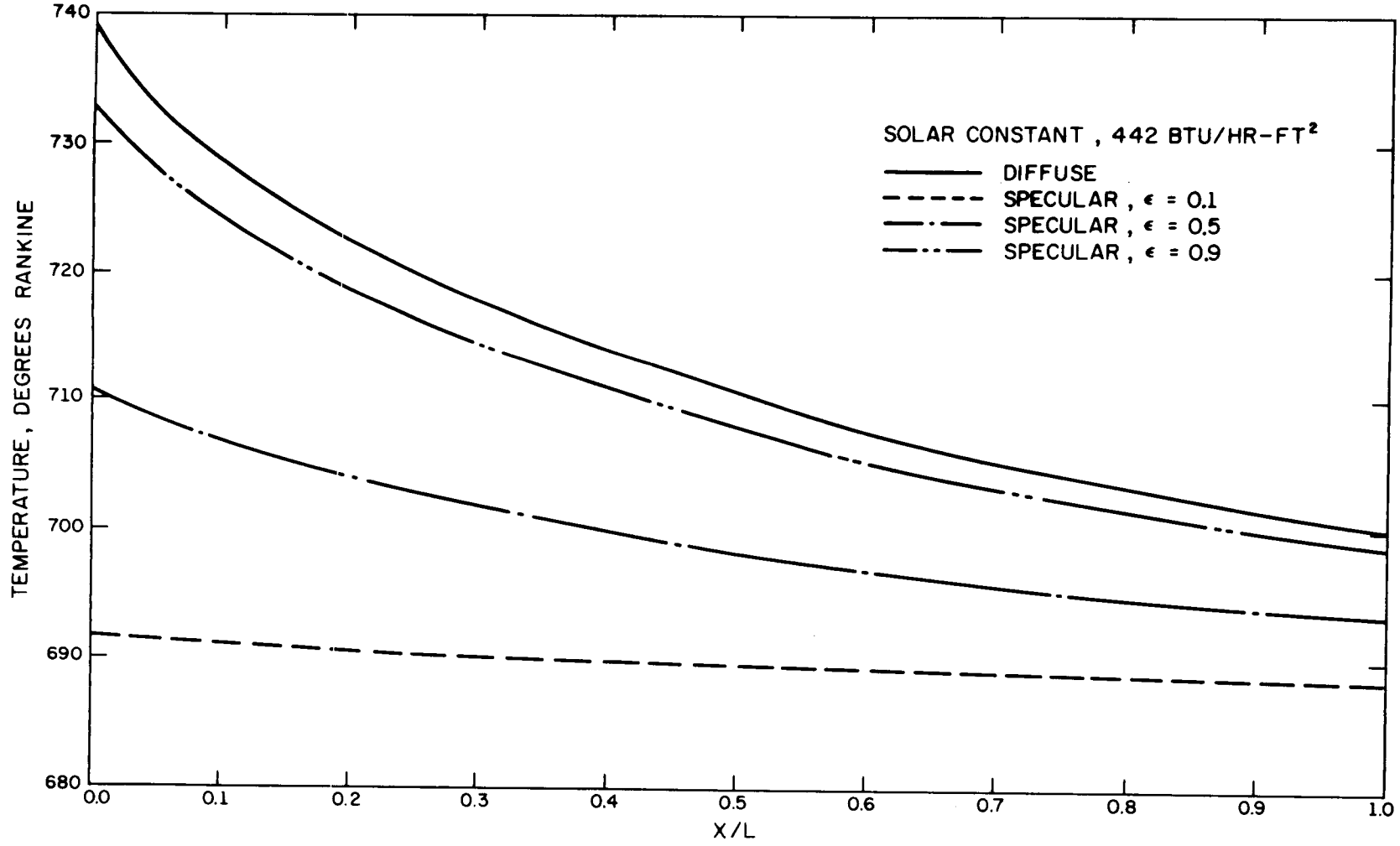

Fig. 23 Equilibrium temperature distributions for the adjoint plate system--gray theory ($\gamma = 120^{\circ}$, $\theta_s = 30^{\circ}$)

increasing values of the opening angle when all other parameters are held fixed. Secondly, the temperature distribution is a monotonically decreasing function of the distance from the apex with the extent of the non-uniformity of temperature from apex to end diminishing with increasing values of the opening angle for selected emissivity.

Of particular interest is the comparison of maximum temperature and equilibrium temperature distributions for the diffusely reflecting and specularly reflecting surfaces at the various opening angles of the system. Turning first to the maximum system temperatures, it may be noted that apex temperatures for the 30° and 90° included angles are independent of the assumed reflection model. Such is not the situation for arbitrary included angles as exemplified by the results for 120°. It may be shown that the corner temperature is independent of whether the surfaces are specularly or diffusely reflecting when the value of the included angle is π/n where n is a positive integer.

The behavior of the equilibrium temperature distributions lends considerable insight into the radiant exchange process. Consider first the results for 120° illustrated in Figure 23. For this value of included angle the contribution of the solar field to the irradiation of the plates is identical for both the diffusely reflecting and specularly reflecting surfaces. Now all reflected energy leaves the opening after a single reflection when the surfaces are specularly reflecting. On the other hand, diffusely reflecting surfaces redistribute the reflected energy uniformily over hemispherical space and hence some of this energy returns to the adjacent surface. Thus, the element at each location of the diffusely reflecting surface experiences a greater incident flux than the corresponding locations on a

specularly reflecting surface. Hence, the diffusely reflecting surface should everywhere exhibit a greater temperature than that of a specularly reflecting surface. This difference in temperature at corresponding locations should increase as the magnitude of the specular reflectance increases. These trends are all evident in Figure 23 . The radiant transfer process for an included angle of 90° has one significant difference from that at 120° which reverses the trends from those of 120°. For an included angle of 90°, the specularly reflecting system experiences an increase in solar flux uniformily over the extent of the surfaces as a result of the image of the solar source in the adjacent surface. That is, an observer stationed on either surface of the specularly reflecting system observes an additional solar source in the adjacent surface with an apparent solar constant which is the product of the surface reflectance and the solar constant of the external field. This increase in local solar flux for the specularly reflecting surfaces should dominate and thereby result in greater irradiation for the specular reflecting system than for the diffusely reflecting surfaces. Since the apparent solar constant increases with the reflectance of the surfaces, the local equilibrium temperatures should increase with increasing reflectance. Figure 22 confirms these observations. The lowest temperatures are achieved by the diffusely reflecting surface with the temperature difference between the diffuse and specular surfaces increasing with increasing values of reflectance. The equilibrium temperature results for an included angle of 30° exhibit both trends evident for 90° and 120° included angles. Near the apex, the increased solar flux due to the five apparent solar sources results in temperatures for the specularly reflecting surfaces which exceed those for the diffusely reflecting surfaces. On the other hand, near the plate

ends where only direct and five times reflected solar energy is incident on a specular surface, the increase in solar flux is not sufficient to exceed the irradiation on a diffuse surface and, consequently, the diffuse surface experiences the higher temperature. The discontinuities in the temperature distribution for the specular surface system evident in Figure 21 are a result of the discontinuities in the locally incident solar flux and neglect of heat conduction in the plates.

A comparison of results to those reported by Plamondon and Landran [9] for the adjoint plate system with diffusely emitting-diffusely reflecting surfaces shows large differences in predicted temperatures. Plamondon and Landran included the wave length dependence in their calculations for some selected materials but used only four elements in their finite difference solution. For an included angle of 30°, the gray diffusely reflecting results reported here exceed those reported for the non-gray analysis by as much as $55^{\circ}R$ for polished aluminum and $185^{\circ}R$ for a surface painted PV-100 white and black. At a value of 60° for the included angle, the gray results were $120^{\circ}R$ lower for the polished aluminum and $140^{\circ}R$ higher for the painted surface. These large differences in predicted temperatures cannot be entirely attributed to the lack of accounting for wave length dependence of properties because the four element finite difference network of Plamondon and Landran is not sufficient for accurate results, especially near the apex where the largest differences in temperature occur. However, even if only half the difference in temperature is attrabuted to non-gray surface property effects, it appears that gray analysis can result in errors as large as almost $100^{\circ}R$ in predicted temperatures.

4.3 Gray Surfaces-Directional Properties

Radiant heat transfer results obtained from a gray surface analysis of the adjoint plate system have been reported in detail in reference [3]. This analysis for specularly reflecting surfaces accounts for the angular dependence of radiative surface properties in the absence of any external radiation field for uniform temperature surfaces. The results of this analysis were compared with the corresponding results determined by analysis which neglects directional property variation ("constant property analysis"). For the range of system parameters studied, local heat transfer derived on the basis of constant property analysis with hemispherical property values gave results of acceptable engineering accuracy except near the apex, where discrepencies as large as a factor of two were observed. Total heat losses evaluated from the simpler constant property analysis were generally within a few percent of those which account for directional property variations. It appears, therefore, that neglect of directional property dependencies in engineering radiant heat transfer calculations for specularly reflecting surfaces is generally justified. Considerable care should be exercised, however, for surfaces which receive major contributions to their irradiation from energy incident at large angles relative to the surface normal.

5.0 Summary and Conclusions

A method of analysis has been presented for the evaluation of radiant heat transfer between engineering materials which accounts for both the spectral and directional character of radiation surface properties. This analysis is being applied to a selected two surface system in the presence of a collimated solar field to determine the local radiant transfer from surfaces with specified temperature distributions and to calculate the local temperature for surfaces with prescribed variation of local radiant heat transfer. Results of this analysis are not yet available but subsidiary investigations in support of the non-gray non-diffuse surface heat transfer study have provided some significant findings. These are summarized here.

The detailed surface property information required to implement the real surface analysis is contained in the spectral bidirectional reflectance of the participating surfaces. As a result of a study of the Davies [6] and Beckmann [7] bi-directional reflectance models it may be concluded that

1. The Davies model is inadequate for the heat transfer study because of its gross violation of the energy conservation requirement in the surface optical roughness range of interest.
2. The Beckmann model is far superior to that of Davies and provides an acceptable description of the spatial description of reflected energy from a roughened metal surface.
3. Sufficient experimental data is not available to adequately evaluate the bidirectional reflectance model.

The approximate directional reflectivity relations derived from electromagnetic theory for $n^2(1 + k^2) >> 1$ provide exceptionally accurate descriptions of the radiation property values of optically smooth uncontaminated surfaces.

Quantitative criteria have been developed which assure certain selected prescribed accuracies in the use of these approximate relations for the evaluation of the polarized reflectivity components as well as the unpolarized reflectivity and hemispherical emissivity.

Intensity distributions determined from the non-gray non-diffuse surface analysis utilizing the Beckmann bi-directional reflectance model have been determined for a simplified version of the original system chosen for analysis. These indicate significant departures from those of diffusely reflecting and specularly reflecting surfaces.

Insufficient results of gray surface analysis for both specularly and diffusely reflecting surfaces are available for the system and environment chosen for study. An effort was initiated to supplement the available results in order that a meaningful comparison to the results of the comprehensive non-gray non-diffuse study could be achieved. Equilibrium temperature distributions determined by the use of gray completely diffuse surface theory show differences in local temperature as large as $185^{\circ}R$ from a recently reported analysis which accounts for the spectral variation of surface properties.

6.0 References

1. A. F. Houchens and R. G. Hering, "Bi-Directional Reflectance of Rough Metal Surfaces," Paper submitted to the American Institute of Aeronautics and Astronautics Thermophysics Specialists Conference, to be held April 17-19, 1967, at New Orleans, La.

2. R. G. Hering and T. F. Smith, " Directional and Hemispherical Surface Radiation Properties," Paper in preparation.

3. R. G. Hering, "Radiative Heat Exchange Between Specularly Reflecting Surfaces with Direction-Dependent Properties," Proceeding Third International Heat Transfer Conference, Vol. 5, pp. 200-206, 1966.

4. R. G. Hering, "Radiative Heat Exchange and Equilibrium Surface Temperatures in a Space Environment," Paper submitted to the American Institute of Aeronautics and Astronautics Fifth Aerospace Sciences Meeting, to be held January 23-25, 1967, at New York, N.Y.

5. F. S. Johnson, "The Solar Constant," Journal of Meteorology, Vol. 11, No. 6, 1954.

6. H. Davies, "The Reflection of Electromagnetic Waves from a Rough Surface," Proc. I.E.E., Part III, Vol. 101, p. 209, 1954.

7. P. Beckmann and A. Spizzichino, "The Scattering of Electromagnetic Waves from Rough Surfaces," The Macmillan Company, New York, 1963.

8. R. C. Birkebak, "Monochromatic Directional Distribution of Reflected Thermal Radiation from Roughened Surfaces," Ph.D. Dissertation, Mechanical Engineering Department, University of Minnesota, Minneapolis, Minnesota, September, 1962.

9. J. A. Plamondon and C. S. Landram, "Radiant Heat Transfer from Non-Gray Surfaces with External Radiation," AIAA, Third Aerospace Sciences Meeting, New York, N.Y., AIAA Paper No. 66-21.